JEM Journal of Experimental Medicine

ARTICLE

Shared pathway of WDFY4-dependent cross-presentation of immune complexes by cDC1 and cDC2

Suin Jo[1], Ray A. Ohara[1], Derek J. Theisen[1], Sunkyung Kim[1], Tiantian Liu[1], Christopher B. Bullock[1,2], Michelle He[1], Feiya Ou[1], Jing Chen[1], Sytse J. Piersma[3,4], J. Luke Postoak[1], Wayne M. Yokoyama[3,5], Michael S. Diamond[1,2,5,6], Theresa L. Murphy[1], and Kenneth M. Murphy[1]

Priming CD8⁺ T cells against tumors or viral pathogens results largely from cross-presentation of exogenous antigens by type 1 conventional dendritic cells (cDC1s). Although monocyte-derived DCs and cDC2s can cross-present in vitro, their physiological relevance remains unclear. Here, we used genetic models to evaluate the role of cDC subsets in presentation of cell-associated and immune complex antigens to CD4⁺ and CD8⁺ T cells in vivo. For cell-associated antigens, cDC1s were necessary and sufficient to prime both CD4⁺ and CD8⁺ T cells. In contrast, for immune complex antigens, either cDC1 or cDC2, but not monocyte-derived DCs, could carry out cross-presentation to CD8⁺ T cells. Mice lacking cDC1 and vaccinated with immune complexes could cross-prime CD8⁺ T cells that were sufficient to mediate tumor rejection. Notably, this cross-presentation mediated by cDC2 was also WDFY4 dependent, similar to cross-presentation of cell-associated antigens by cDC1. These results demonstrate a previously unrecognized activity of WDFY4 in cDC2s and suggest a cross-presentation pathway shared by cDC subsets.

Introduction

Conventional dendritic cells (cDCs) are APCs that specialize in priming of naive T cells (Liu and Nussenzweig, 2010). Currently, two major subsets of cDCs are recognized, the type 1 cDC (cDC1) and cDC2 (Guilliams et al., 2014), which are thought to exert distinct functions in forming immunity to various pathogens (Durai and Murphy, 2016). Their distinct roles have been linked to intrinsic biases in priming of CD8⁺ and CD4⁺ T cells based on differences in antigen processing for MH class I (MHC-I) and MHC-II molecules. Early studies suggested such differences in cross-presentation (Carbone and Bevan, 1990), finding that CD8α⁺, but not CD8α⁻, cDCs were capable of processing cell-associated antigens for CD8⁺ T cell activation (den Haan et al., 2000). Targeting antigen conjugated to antibodies that bind receptors expressed by cDC1 or cDC2 showed that these subsets have an intrinsic bias, with cDC1 favoring antigen processing for MHC-I and cDC2 favoring antigen processing for MHC-II (Dudziak et al., 2007). Consistent with these experiments, studies of mice lacking cDC1 showed that cDC1 are predominantly responsible for in vivo cross-presentation of exogenously acquired antigens via MHC-I in response to tumors and viral infections (Hildner et al., 2008; Durai et al., 2019).

However, in addition to intrinsic biases that cDC subsets exhibit, the form of antigen itself impacts presentation by cDC1 and cDC2. For example, for tumor-derived antigens, cDC1 are also the primary subset responsible for in vivo antigen presentation by MHC-II molecules to CD4⁺ T cells (Ferris et al., 2020). This capacity may arise from expression of cDC1-specific receptors, such as C-type lectin domain family 9, that mediate efficient capture of necrotic tumor cells, providing cDC1 with an advantage over cDC2 for acquiring tumor-derived antigens (Sancho et al., 2009). Conversely, cDC2 can also cross-present antigens, at least in vitro, particularly when provided as soluble protein or as an immune complex (IC) (den Haan and Bevan, 2002; Kamphorst et al., 2010). In vitro cross-presentation by

[1]Department of Pathology and Immunology, Washington University in St. Louis School of Medicine, St. Louis, MO, USA; [2]Department of Medicine, Washington University in St. Louis, School of Medicine, St. Louis, MO, USA; [3]Division of Rheumatology, Department of Medicine, Washington University School of Medicine, St. Louis, MO, USA; [4]Siteman Cancer Center, Washington University School of Medicine, St. Louis, MO, USA; [5]The Andrew M. and Jane M. Bursky Center for Human Immunology and Immunotherapy Programs, Washington University in St. Louis, School of Medicine, St. Louis, MO, USA; [6]Department of Molecular Microbiology, Washington University in St. Louis, School of Medicine, St. Louis, MO, USA.

Correspondence to Kenneth M. Murphy: kmurphy@wustl.edu

S. Kim's current affiliation is Department of Microbiology, Ajou University School of Medicine, Suwon, South Korea. K.M. Murphy is a lead contact.

© 2025 Jo et al. This article is distributed under the terms as described at https://rupress.org/pages/terms102024/.

Check for updates

Downloaded from http://rupress.org/jem/article-pdf/222/4/e20240955/1938722/jem_20240955.pdf by guest on 08 May 2026

cDC2 is mediated by distinct receptors compared with cDC1, such as Fcγ receptors (Baker et al., 2011; Boross et al., 2014; Ho et al., 2017). However, the relevance of cross-presentation by cDC2 in vivo has not been established because previous studies were unable to exclude the contribution of cDC1 in priming of T cell responses.

To address this question, we examined T cells responses in mice having either exclusively cDC1 or cDC2, in which priming by various antigens can occur by only one cDC subset. Basic leucine zipper transcription factor (*Batf3*$^{-/-}$) mice lack cDC1 due to defective progenitor commitment (Hildner et al., 2008) but can restore cDC1 development under certain conditions due to compensation by *Batf* (Tussiwand et al., 2012). However, we previously developed mice with a deletion of the interferon regulatory factor 8 (*Irf8*) +32 kb enhancer (hereafter Δ32 mice), which lack cDC1 completely without compensation (Durai et al., 2019). Separately, we also developed mice with deletions of the three CCAAT-enhancer–binding protein α–binding sites in the zinc-finger E-box–binding homeobox 2 –165 kb enhancer (hereafter Δ1+2+3 mice), which lack cDC2 due to failure in pre-cDC2 specification (Liu et al., 2022a). We previously used these models to confirm the role of cDC1 in CD8$^+$ T cell responses to tumors and several viruses (Durai et al., 2019; Ferris et al., 2020) and the requirement of cDC2 in Th2 responses to helminths (Liu et al., 2022a). However, no study has used these mice to compare both the requirement and sufficiency for cDC subsets in priming CD4$^+$ and CD8$^+$ T cells responses to a variety of forms of antigen.

The cellular mechanism of cross-presentation is complex and controversial due to variations between in vitro and in vivo studies and the use of different cell substrates and forms of antigen (Ohara and Murphy, 2023a; Blander, 2023). We previously reported that cross-presentation of cell-associated antigens by cDC1 in vivo requires WD repeat and FYVE domain–containing 4 (WDFY4), a Beige and Chediak-Higashi domain–containing protein (Theisen et al., 2018; Ohara and Murphy, 2023b). While the mechanism of WDFY4 in cross-presentation remains unknown, several other Beige and Chediak-Higashi domain–containing proteins function by regulating vesicular trafficking (Cullinane et al., 2013). WDFY4 is highly expressed in cDC1 and cDC2, less in B cells, and absent in most other cells (Theisen et al., 2018). Unlike cross-presentation of cell-associated antigen by cDC1, cross-presentation of soluble antigen by cDC2 does not require WDFY4 (Theisen et al., 2018).

In this study, we used Δ32 mice and Δ1+2+3 mice to determine in vivo requirement and sufficiency for priming of CD4$^+$ and CD8$^+$ T cell responses to various forms of antigen. We find that cDC2 are sufficient for cross-presentation of antibody–antigen ICs and for induction of CD8$^+$ T cell responses that protect against immunogenic tumors, which normally requires cDC1. Notably, cDC2 cross-presentation of ICs is WDFY4 dependent, unlike cross-presentation of soluble antigens. These results suggest a novel role for cDC2 in priming of CD8$^+$ T cells and demonstrate that receptor-mediated antigen capture may favor cross-presentation by a more efficient, WDFY4-dependent processing pathway in cDC subsets.

Results

Characterization of cDC1- and cDC2-deficient mouse models

We first confirmed that Δ32 mice and Δ1+2+3 mice lack cDC1 and cDC2, respectively (Fig. S1, A–D) (Durai et al., 2019; Liu et al., 2022a). Δ32 mice retain pre-cDC1 in the bone marrow (BM), lack mature cDC1, and have approximately twofold more splenic cDC2 than WT mice (Fig. S1, A–D). In contrast, Δ1+2+3 mice lack pre-cDC2 and mature cDC2 and have approximately twofold more splenic cDC1 than WT mice. To determine if the residual cDC subsets in the Δ1+2+3 and Δ32 mice reflected their normal counterparts, we performed bulk RNA-sequencing (RNA-seq) analysis of cDC1 and cDC2 from WT, Δ1+2+3, and Δ32 mice (Fig. 1 A). cDC1 from WT and Δ1+2+3 clustered together in principal component analysis plot, whereas cDC2 from WT and Δ32 mice cluster together. Further, cDC1 and cDC2 from WT mice show a large number of differentially expressed genes, as expected. However, there were few differentially expressed genes in cDC1 between WT and Δ1+2+3 mice, or in cDC2 between WT and Δ32 mice (Fig. 1 A), indicating no substantive transcriptional differences between corresponding cDC subsets in WT, Δ32, and Δ1+2+3 mice. These results validate the use of these models for testing the sufficiency of cDC1 and cDC2 for presentation of various forms of antigens in vivo.

cDC1 are necessary and sufficient to prime CD8$^+$ T cells to cell-associated antigen in vivo

cDC1 are the principal APC for priming both CD4$^+$ and CD8$^+$ T cells in response to cell-associated tumor antigens (Ferris et al., 2020). Some studies have suggested that cDC1 may require monocytes or cDC2 for antigen acquisition or functional activation (Ruhland et al., 2020; Jakubzick et al., 2013, 2017; Rawat et al., 2023). To test this first for CD8$^+$ T cell responses, we generated Abelson-membrane–associated OVA (mOVA), a tumor cell expressing mOVA but lacking MHC-I expression. We used freeze-thawed Abelson-mOVA cells as one source of necrotic tumor cell-associated antigen. OT-I T cells proliferated in response to Abelson-mOVA that was presented by splenic cDC1 (Fig. 1, B and C) or by BM-derived cDC1 (Fig. S2, A and B) at levels similar to heat-killed *Listeria monocytogenes*–expressing OVA (HKLM-OVA), a different cell-associated antigen used previously (Kretzer et al., 2016; Theisen et al., 2018). By contrast, OT-I did not proliferate in response to either Abelson-mOVA or HKLM-OVA presented by splenic or BM-derived cDC2 (Fig. 1, B and C; and Fig. S2, A and B). As a control, OT-I proliferated in response to soluble OVA (sOVA) presented either by cDC1 or cDC2, as expected (Kretzer et al., 2016; Theisen et al., 2018) (Fig. 1, B and C; and Fig. S2, A and B). These results indicate that Abelson-mOVA is a valid source of cell-associated antigen to examine cross-presentation by APCs without trogocytosis of self-loaded peptide–MHC-I complexes from tumor to the cell surface of APCs.

To test if cDC1 require cDC2 or monocytes to acquire cell-associated antigens, we adoptively transferred OT-I cells into WT, Δ32, *Wdfy4*$^{-/-}$, or Δ1+2+3 mice and measured OT-I proliferation after injection of freeze-thawed necrotic Abelson-mOVA cells (Fig. 1, D and E; and Fig. S2 G). OT-1 proliferated in WT mice, but not in Δ32 or *Wdfy4*$^{-/-}$ mice, which lack cDC1 or the

Downloaded from http://rupress.org/jem/article-pdf/222/4/e20240955/1938722/jem_20240955.pdf by guest on 08 May 2026

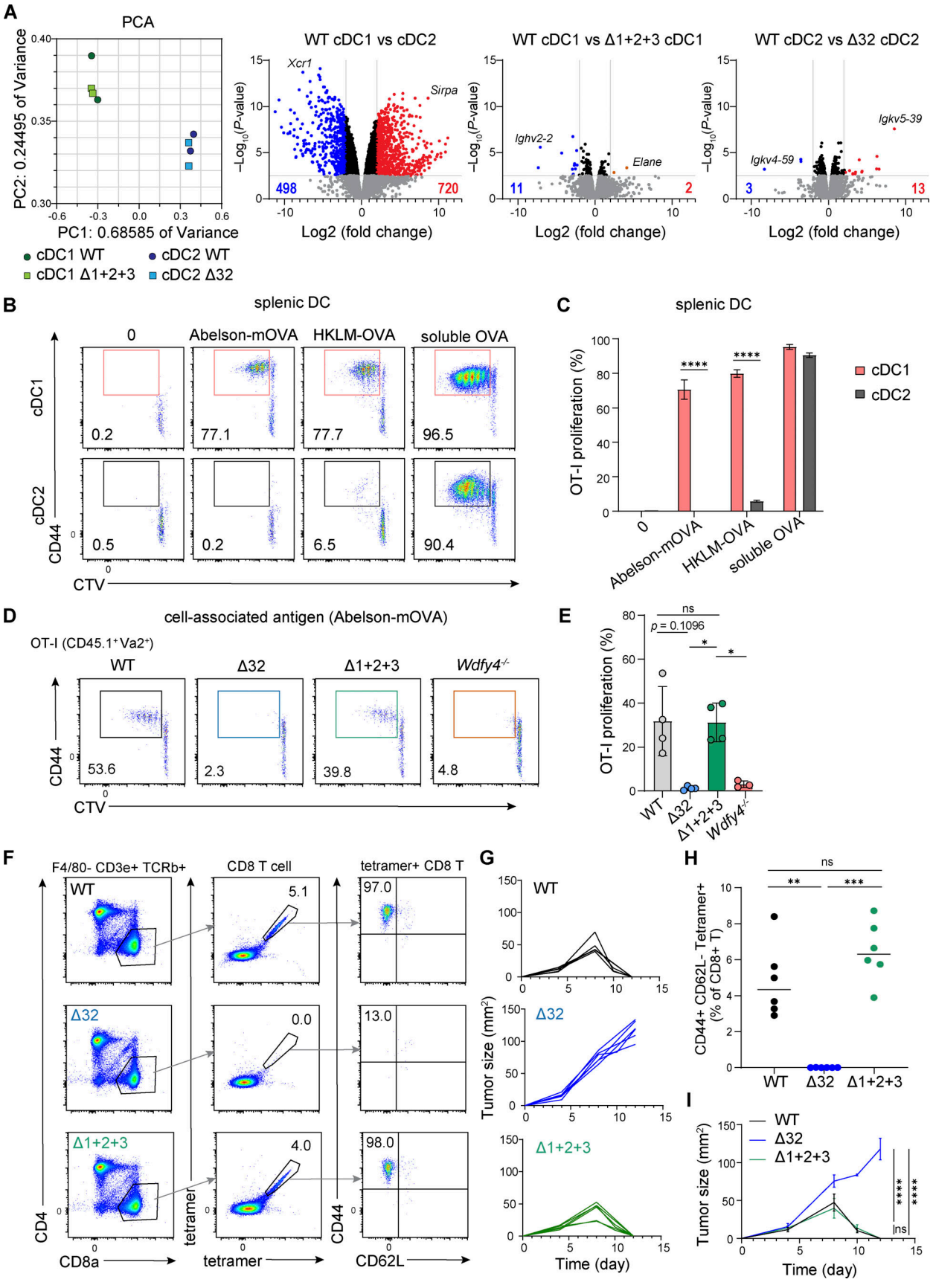

Figure 1. **cDC1 are necessary and sufficient for priming CD8⁺ T cells with cell-associated antigen. (A)** Principal component analysis by all expressed mRNAs of splenic cDC1s and cDC2s from WT, Δ32, and Δ1+2+3 mice. PC1: 0.68585 of variance. PC2: 0.24495 of variance. Volcano plots of differentially

Downloaded from http://rupress.org/jem/article-pdf/222/4/e20240955/1938722/jem_20240955.pdf by guest on 08 May 2026

expressed genes as the Log_2 (fold change) over $-Log_{10}$ (P value). (Left) cDC1 and cDC2 in WT mice. Data are represented as two biologically independent samples. (Middle) cDC1 in WT and *Δ1+2+3* mice. (Right) cDC2 in WT and *Δ32* mice. Transcripts with significant changes in expression are highlighted in red (increased) or blue (decreased). **(B)** In vitro proliferation of 2.5×10^4 OT-I cells cultured with 10^4 splenic cDC1 or cDC2 alone or with 2.5×10^4 Abelson-mOVA cells, 10^8 HKLM-OVA, or sOVA (100 µg/ml) as indicated. Numbers represent the percent of cells in the indicated gates. **(C)** Percent OT-I proliferation from B averaged for two independent experiments. Data are represented as mean values ± SD. Multiple *t* tests. ****P < 0.0001. **(D and E)** In vivo proliferation of OT-I in WT, *Δ32*, *Δ1+2+3*, and *Wdfy4*$^{-/-}$ mice on day 3 after immunization with 3.3×10^5 Abelson-mOVA cells. Data are represented as mean values ± SD of pooled biologically independent samples from two independent experiments. *n* = 4 for WT, Δ32, and Δ1+2+3; *n* = 3 for *Wdfy4*$^{-/-}$ mice. ns = not significant; *P < 0.05. **(F)** Two-color histograms for splenocytes from WT, *Δ32*, and *Δ1+2+3* mice on day 12 after injection of 10^6 1956-mOVA cells. CD8$^+$ T cells were analyzed for the frequency of K^b-SIINFEKL tetramer staining. Pregating is indicated above the histograms. Numbers indicate the percentage of cells in the indicated gates. **(G)** Frequencies of K^b-SIINFEKL tetramer–positive CD8$^+$ T cells from mice described in F. *n* = 6 for WT and Δ32; *n* = 5 for Δ1+2+3 mice. **(H and I)** Individual or averaged tumor growth in WT, *Δ32*, and *Δ1+2+3* mice implanted with 10^6 1956-mOVA cells. *n* = 6 for each genotype. **(E and H)** Brown–Forsythe and Welch ANOVA with Dunnett's T3 multiple comparisons test. **P < 0.01; ***P < 0.001. **(I)** Two-way ANOVA with Tukey's multiple comparisons test. ns = not significant; WT versus Δ1+2+3. ****P < 0.0001; WT versus Δ32. ****P < 0.0001; Δ32 versus Δ1+2+3. PCA: Principal component analysis.

capacity for cross-presentation, respectively. Notably, OT-I proliferated in Δ1+2+3 mice to a comparable extent as in WT mice, indicating that cDC2, monocytes, and monocyte-derived cells are not required for cDC1 in priming of CD8$^+$ T cells against tumor-derived antigens. Rather, cDC1 are both necessary and sufficient for this function.

cDC1 are sufficient for anti-tumor CD4$^+$ and CD8$^+$ T cell priming in vivo

We next tested these results in the context of an endogenous CD8$^+$ T cell repertoire. We compared the antigen-specific endogenous CD8$^+$ T cell response against the 1956 tumor cell line–expressing mOVA (1956-mOVA) fibrosarcoma (Matsushita et al., 2012; Theisen et al., 2019), which expresses membrane-bound OVA with normal MHC-I expression, in WT, Δ32, and Δ1+2+3 mice (Fig. 1, F–I). As expected, WT mice robustly expanded SIINFEKL-H2K^b tetramer–positive CD8$^+$ T cells in response to 1956-mOVA after tumor implantation (Ferris et al., 2020; Wu et al., 2022) and cleared tumor by day 12. In contrast, Δ32 mice did not expand SIINFEKL-H2K^b tetramer–positive CD8$^+$ T cells and failed to reject 1956-OVA tumors. Δ1+2+3 mice, however, expanded SIINFEKL-H2K^b tetramer–positive CD8$^+$ T cells as effectively as WT mice and rejected tumors comparably to WT mice. These results show that priming of endogenous anti-tumor CD8$^+$ T cells is normal in Δ1+2+3 mice even in the absence of cDC2 and monocyte-derived cells. Since CD8$^+$ T cell priming against 1956-mOVA and tumor rejection require CD4$^+$ T cell help (Ferris et al., 2020), these results also imply that CD4$^+$ T cell priming against tumor-associated antigens can occur in the absence of cDC2 or monocyte-derived cells.

Recent studies using Batf3$^{-/-}$ mice reported that cDC2 can acquire an activation state, called inflammatory cDC2 (Bosteels et al., 2020) or ISG$^+$ cDC2 (Duong et al., 2022), capable of priming CD8$^+$ T cells in response to infection by influenza A, pneumonia virus in mice, and tumors. We infected WT and Δ32 mice with Ross River virus (RRV) (Haist et al., 2021; Liu et al., 2022b; Shabman et al., 2008). After 1 day, OT-I cells were transferred, and mice were immunized on day 2 with dead Abelson-mOVA tumor cells. In both WT and Δ32 mice, we observed the emergence of a CD11c$^+$ MHCII$^+$ FcεR1 α monoclonal antibody CD64$^+$ cells (Bosteels et al., 2020) both in spleen and popliteal LNs in mice infected with RRV but not in uninfected mice (Fig. S2 C). Importantly, Δ32 mice infected with RRV showed a substantial OT-I proliferation in response to Abelson-mOVA immunization, while uninfected Δ32 mice showed little to no OT-I proliferation (Fig. S2 D). These results agree with the previous studies suggesting that inflammatory cDC2 are capable of CD8 T cell priming.

Both cDC1 and cDC2 can cross-prime CD8$^+$ T cells to IC in vivo

Several in vitro studies have suggested that both cDC1 and cDC2 can cross-present antigen offered in the form of antigen–antibody complexes (den Haan and Bevan, 2002; van Montfoort et al., 2007; Baker et al., 2011; Boross et al., 2014; Ho et al., 2017). In contrast, another study found that cDC2 offered FcγR-targeting antigens that were able to prime CD4$^+$ T cells, but not CD8$^+$ T cells (Lehmann et al., 2017). To address this question in vivo, we first re-evaluated the previous in vitro finding. Here, we found that cDC2 are capable of cross-presentation of OVA–antibody complexes in vitro (Fig. 2, A and B). In doses between 1 and 3 µg/ml of sOVA alone, OT-I T cells did not proliferate in the presence of cDC1 or cDC2, whereas substantial proliferation was observed with sOVA preincubated with anti-OVA polyclonal antibody (OVA-ICs) (Fig. 2, A and B). To test whether cDC2 can cross-present immune-complexed OVA (OVA-IC) in vivo, we examined OT-I proliferation after adoptive transfer of OT-I cells into WT, Δ32, and Δ1+2+3 mice that were subsequently immunized with either 1 µg of sOVA or OVA-IC (Fig. 2, C and D; and Fig. S2 G). Immunization with sOVA alone failed to induce OT-I proliferation in any genotype of mice, whereas immunization with OVA-IC induced strong OT-I proliferation in all genotypes, including Δ32 mice (Fig. 2, C and D; and Fig. S2 G).

Conceivably, cDC2 cross-presentation might extend to cell-associated antigens via Fc receptor binding. To test this, we generated antibody-coated cellular antigens. Abelson-mOVA, which express membrane-bound OVA on the cell surface via a linker, was preincubated with polyclonal anti-OVA antibody at 37°C, similar to the OVA-IC preparation. We confirmed antibody binding to the dead Abelson-mOVA by flow cytometry (Fig. S2 E). Nonetheless, this anti-OVA-coated Abelson-mOVA was not cross-presented by splenic cDC2 to OT-I T cells (Fig. 2 E and Fig. S2 F). Consistent with this in vitro result, Δ32 mice immunized with same antigen did not induce OT-I proliferation (Fig. 2, F and G), indicating that receptor engagement is insufficient for cDC2 cross-presentation of cellular antigen.

Conceivably, the OT-I proliferation induced by OVA-IC in Δ32 mice could result from cross-presentation by other APCs,

Downloaded from http://rupress.org/jem/article-pdf/222/4/e20240955/1938722/jem_20240955.pdf by guest on 08 May 2026

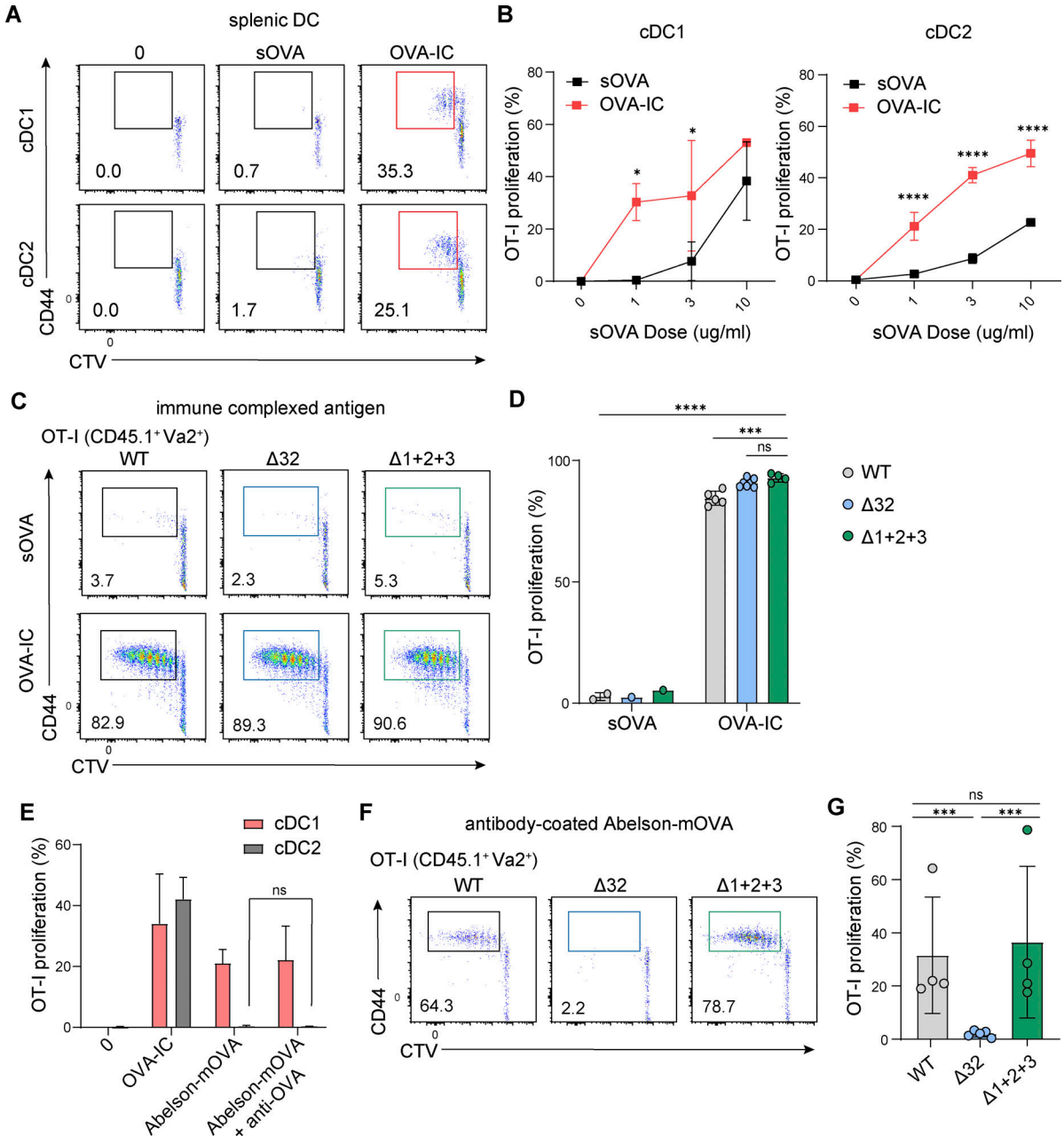

Figure 2. **cDC1 are dispensable for in vivo cross-priming with IC. (A and B)** In vitro proliferation of OT-I cultured with splenic cDC1 or cDC2 alone (0) or with 1 µg/ml of sOVA or OVA-IC (A) or with the indicated doses of sOVA or OVA-IC (B). Data shown are representative of two independent experiments. **(B)** Two-way ANOVA with Sidak's multiple comparisons test, with a single pooled variance. *P < 0.05; ****P < 0.0001. **(C)** In vivo OT-I proliferation in WT, *Δ32*, and *Δ1+2+3* mice on day 3 after intravenous immunization with 1 µg sOVA or 1 µg sOVA with anti-OVA antibody (OVA-IC). **(D)** Frequencies of OT-I proliferation from mice in C. Two-way ANOVA with Tukey's multiple comparisons test. ns = not significant; ***P < 0.001; ****P < 0.0001. **(E)** In vitro proliferation of OT-I cultured with splenic cDC1 or cDC2 alone (0), 1 µg/ml of OVA-IC, 25,000 Abelson-mOVA, or 25,000 Abelson-mOVA preincubated with anti-OVA antibody. Unpaired *t* test. ns = not significant. **(F)** In vivo OT-I proliferation in WT, *Δ32*, and *Δ1+2+3* mice on day 3 after intravenous immunization with 330,000 Abelson-mOVA preincubated anti-OVA antibody. **(G)** Frequencies of OT-I proliferation from mice in F. Two-way ANOVA with Tukey's multiple comparisons test. ns = not significant; ***P < 0.001.

such as macrophages or monocyte-derived DCs (moDCs). Indeed, MER proto-oncogene, tyrosine kinase (MerTK$^+$) moDCs or macrophages (Gautier et al., 2012; Min et al., 2018) can cross-present OVA-IC in vitro (Fig. 3, A and B). To test if these cells mediate cross-presentation of OVA-ICs in Δ32 mice, we crossed $\beta2m^{fl/fl}$ mice (Bern et al., 2019; Ferris et al., 2020) with *Cd11c*-Cre$^+$ mice (Fig. S3). In these mice, H2-K^b and H2-D^b expression is eliminated on majority of cDC1s and cDC2s but remains expressed on B cells, pDCs, and MerTK$^+$ macrophages and moDCs (Fig. S3, A–G). Notably, CD11c-Cre$^+$ $\beta2m^{fl/fl}$ mice showed a 96% reduction in OT-I proliferation in vivo in response to OVA-IC (Fig. 3, C and D). As a control, germline MHC-I deficiency (MHC-I TKO) also caused complete loss of OT-I proliferation in response to OVA-IC in vivo (Fig. S3 H).

Downloaded from http://rupress.org/jem/article-pdf/222/4/e20240955/1938722/jem_20240955.pdf by guest on 08 May 2026

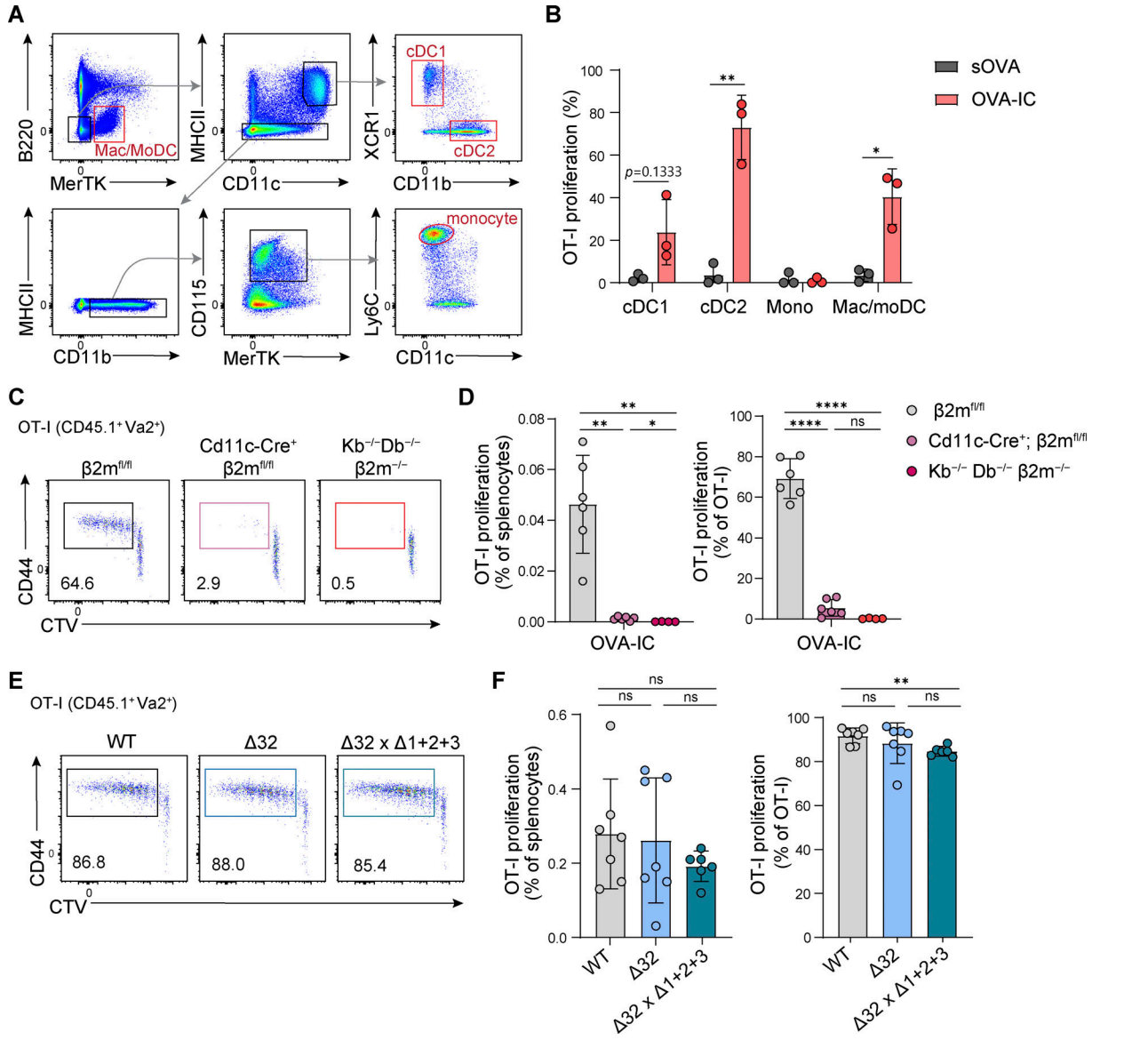

Figure 3. **In vivo cross-priming with IC requires cDC1 or cDC2. (A)** Sorting strategy for cDC1, cDC2, monocytes, and macrophage/moDCs. **(B)** In vitro proliferation of OT-I cultured with the indicated APC and either 1 µg/ml of sOVA or OVA-IC. Data are represented as mean values ± SD combined from three independent experiments. Multiple *t* tests. *P < 0.05; **P < 0.01. **(C)** In vivo OT-I proliferation in β2m$^{fl/fl}$, CD11c-Cre^{+}; β2m$^{fl/fl}$, or MHC-I TKO (Kb$^{-/-}$; Db$^{-/-}$; and β2m$^{-/-}$) mice 3 days after intravenous immunization with 1 µg OVA-IC. **(D)** Frequencies of OT-I proliferation from mice in C. Data are represented as mean values ± SD of pooled biologically independent samples from two independent experiments (n = 6 for β2m$^{fl/fl}$ and CD11c-Cre^{+}; β2m$^{fl/fl}$; n = 4 for MHC-I TKO mice). ns = not significant; *P < 0.05; **P < 0.01; ****P < 0.0001. **(E)** In vivo OT-I proliferation in WT, *Δ32*, and *Δ32 × Δ1+2+3* mice on day 3 after intravenous immunization with 1 µg OVA-IC. Data represent mean ± SEM of pooled biologically independent samples from two independent experiments (n = 7 for WT and *Irf8* Δ 32 mice; n = 6 for *Δ32 × Δ1+2+3* mice). **(D and F)** Brown–Forsythe and Welch ANOVA with Dunnett's T3 multiple comparisons test. ns = not significant; **P < 0.01.

Finally, we tested whether cDC2s alone are sufficient for OVA-IC cross-presentation to OT-I in vivo. We crossed Δ32 with Δ1+2+3 mice to generate Δ32 × Δ1+2+3 mice that lack cDC1, monocytes, and all monocyte-derived cells but retain cDC2s as previously described (Liu et al., 2022a). In these mice, immunization with OVA-IC continued to induce strong OT-I proliferation comparable with Δ32 mice (Fig. 3, E and F), demonstrating that cDC2s are sufficient for cross-presentation of OVA-IC to CD8^{+} T cells in vivo. Δ32 × Δ1+2+3 mice had a decreased OT-I proliferation compared with WT mice (Fig. S3 I), conceivably due to the absence of monocytes or monocyte-derived cells. In summary, in vivo cross-presentation of OVA-IC can be carried out in mice having only cDC1 (Δ1+2+3) (Fig. 2, C and D) and in mice having only cDC2 (Δ32 × Δ1+2+3) (Fig. 3, E and F), indicating that both cDC1 and cDC2 can autonomously perform this function.

cDC1 are poor APCs for priming CD4^{+} T cells against IC in vivo

We next asked whether presentation to CD4^{+} T cells by cDCs requires help from other APCs. First, we assessed OT-II proliferation in WT, Δ32, and Δ1+2+3 mice in response to 1956-mOVA

Downloaded from http://rupress.org/jem/article-pdf/222/4/e20240955/1938722/jem_20240955.pdf by guest on 08 May 2026

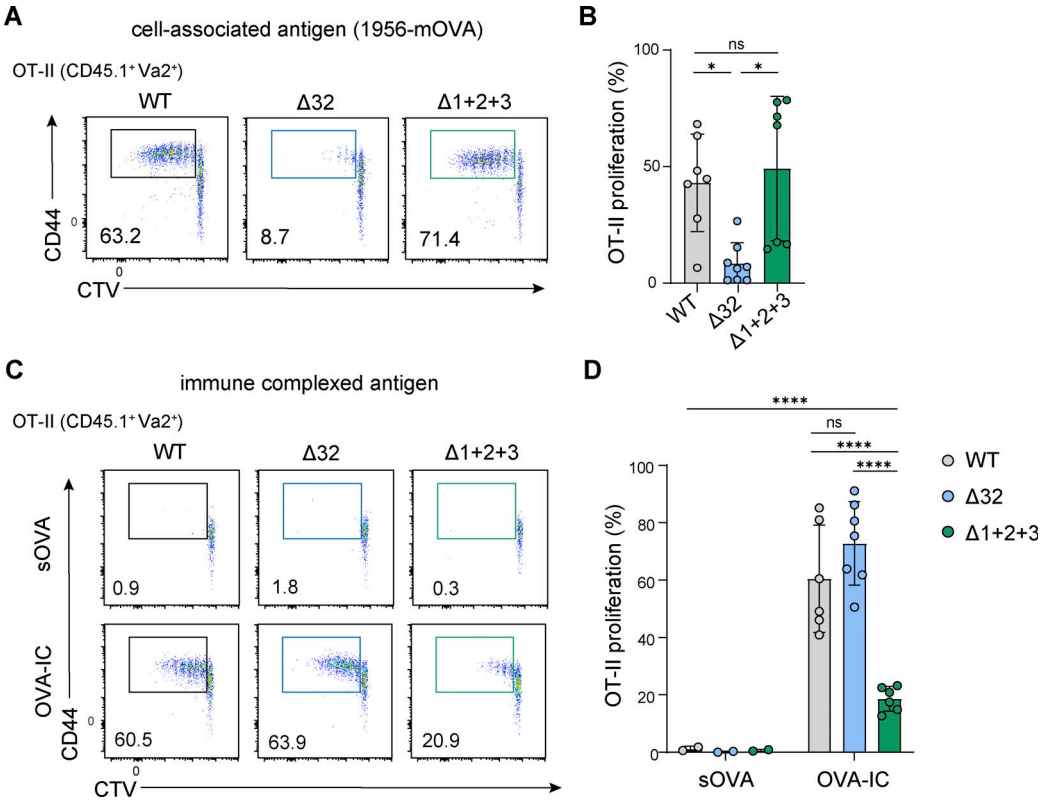

Figure 4. **cDC2 are superior to cDC1 for IC for MHC-II presentation. (A)** In vivo OT-II proliferation 3 days after adoptive transfer into WT, *Δ32*, and *Δ1+2+3* mice bearing 1956-mOVA tumors. 10^6 1956-mOVA cells were subcutaneously injected into mice two days before the OT-II transfer. **(B)** Frequencies of OT-II proliferation of mice described in A. Data are represented as mean values ± SD of pooled biologically independent samples from two independent experiments (*n* = 7 for WT and *Δ1+2+3*; *n* = 8 *Irf8* Δ 32 mice). ns = not significant; *P < 0.05. **(C)** In vivo OT-II proliferation in WT, *Δ32*, and *Δ1+2+3* mice on day 3 after intravenous immunization with 1 µg of sOVA or OVA-IC. **(D)** Frequencies of OT-II proliferation from mice described in C. Data represent mean ± SEM of pooled biologically independent samples from two independent experiments. **(B)** Brown–Forsythe and Welch ANOVA with Dunnett's T3 multiple comparisons test. **(D)** Two-way ANOVA with Sidak's multiple comparisons test, with a single pooled variance. ns = not significant; ****P < 0.0001.

fibrosarcoma (Fig. 4, A and B; and Fig. S2 I). We found strong OT-II proliferation in WT and Δ1+2+3 mice, but not in Δ32 mice, suggesting that CD4+ T cell priming to tumor-derived antigens relies on the presence of cDC1. Since Δ1+2+3 lack both cDC2 and monocyte-derived cells, these results also suggest cDC1 do not rely on accessory functions provided by cDC2, monocytes, or moDCs. Next, we assessed presentation of sOVA and OVA-IC to OT-II in WT, Δ32, and Δ1+2+3 mice (Fig. 4, C and D; and Fig. S2 J). We found strong OT-II proliferation in WT and Δ32 mice, but not in Δ1+2+3 mice, in response to OVA-IC immunization. As a negative control, OT-II proliferation was not induced by sOVA alone in any mouse genotype. Thus, cDC1 are necessary for in vivo presentation of cell-associated antigens to CD4+ T cells but dispensable for antigens derived from ICs.

OVA-IC elicits cDC1-independent endogenous anti-tumor CD8+ T cell response in vivo

cDC1 are normally required for tumor rejection because tumor-associated antigens are not cross-presented by cDC2 (Ferris et al., 2020). Since cDC2 can cross-present antibody-complexed antigen, we evaluated whether cDC2 could also prime CD8+ T cells and support tumor rejection when tumor-derived antigens are delivered in an IC form. To test this, we immunized WT and Δ32 mice with adjuvant (CpG and anti-CD40 antibody) and either sOVA or OVA-IC. After 5 days, 1956-mOVA was implanted subcutaneously, and tumor growth and clearance were assessed (Fig. 5 A and Fig. S4 A). Using sOVA, tumors engrafted and were rejected by all WT mice but failed to be rejected in all Δ32 mice. Using OVA-IC, tumor engraftment was uniformly prevented in both WT mice and Δ32 mice. Since cDC1 development is restored in *Batf3*$^{-/-}$ mice under certain conditions (Tussiwand et al., 2012), we checked for cDC1 restoration by treatment with OVA-IC and adjuvant during tumor growth in Δ32 mice (Fig. 5 B). We found no evidence that these conditions led to cDC1 restoration. In addition, immunization with OVA-IC in CFA also led complete clearance of 1956-mOVA tumors in all Δ32 mice (Fig. 5 C). Importantly, CD8+ T cell depletion restored growth of tumors in Δ32 mice immunized with OVA-IC and CFA (Fig. 5 C and Fig. S4 B). In summary, OVA-IC immunization can induce cDC1-independent but CD8+ T cell–dependent anti-tumor responses in Δ32 mice.

Cross-presentation of OVA-IC by both cDC1 and cDC2 is WDFY4 dependent

We previously identified WDFY4 as a requirement for cross-presentation of cell-associated antigen by cDC1 but reported no

Downloaded from http://rupress.org/jem/article-pdf/222/4/e20240955/1938722/jem_20240955.pdf by guest on 08 May 2026

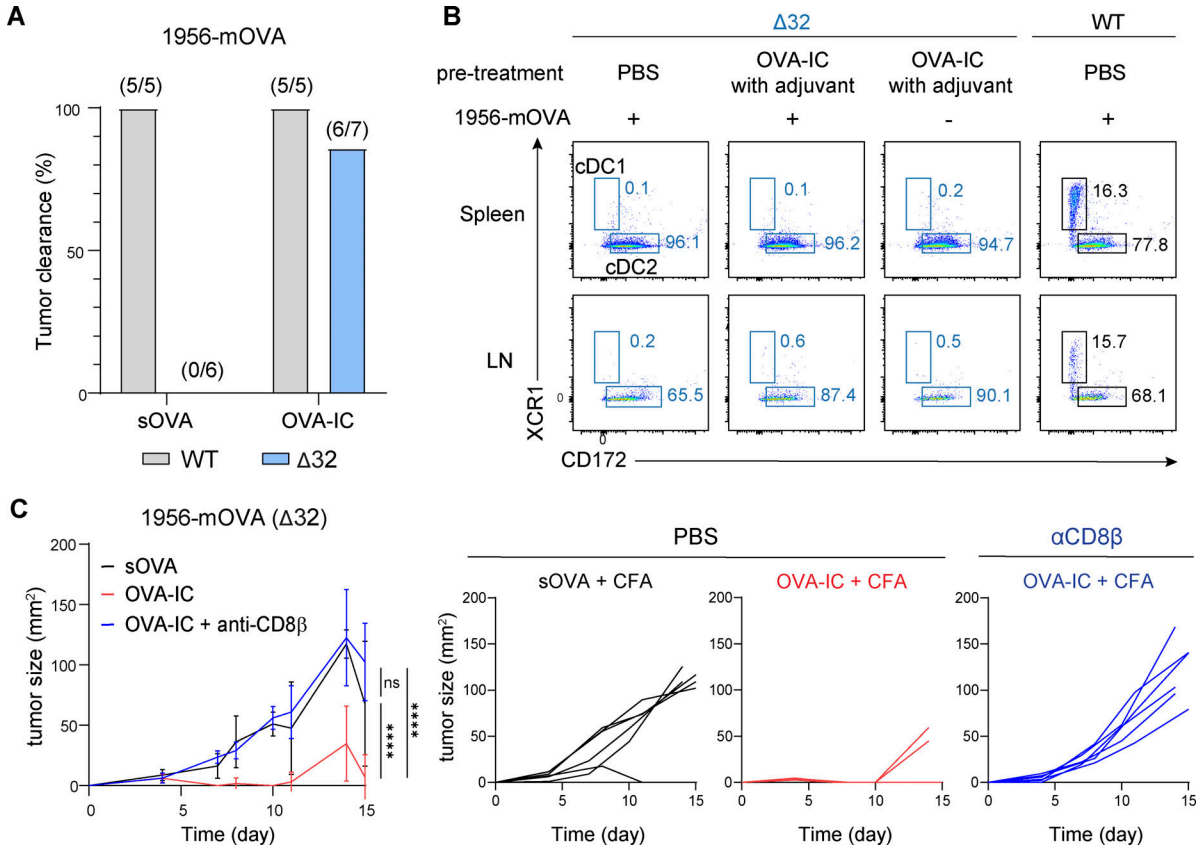

Figure 5. **Immunization with ICs induces anti-tumor immunity in *Irf8* Δ32 mice. (A)** WT and Δ32 mice intravenously immunized with CpG + anti-CD40 antibody and either 5 µg of sOVA or OVA-IC. After 5 days, 10^6 1956-mOVA was implanted subcutaneously, and tumor clearance was measured until day 15. Data are pooled biologically independent samples from three independent experiments. **(B)** cDCs were evaluated in spleen and tumor draining LN in WT or Δ32 mice with the indicated conditions of immunization and tumor implantation. Two-color histograms are pregated as $B220^-$ $CD11c^+$ $MHC\text{-}II^+$ cells. Shown are two-color histograms for XCR1 and CD172 expression. Numbers are the percentage of cells in the indicated gates. **(C)** Δ32 mice treated with i.p. PBS or i.p. anti-CD8β antibody to deplete $CD8^+$ T cells. Next day, mice were subcutaneously immunized with CFA and either 5 µg of sOVA or OVA-IC. After 5 days, mice were subcutaneously implanted with 10^6 1956-mOVA cells and tumor growth monitored for 15 days. (Left) tumor growth. Data are represented as mean values ± SD of pooled biologically independent samples from two independent experiments (n = 6 for each genotype). Two-way ANOVA with Tukey's multiple comparisons test. ns = not significant; ****P < 0.0001.

impact of WDFY4 on antigen presentation by cDC2 (Theisen et al., 2018). However, WDFY4 is also highly expressed in cDC2 at levels similar to that in cDC1 (Theisen et al., 2018). Therefore, we asked whether cross-presentation of OVA-IC by cDC1 and cDC2 requires WDFY4. As we previously reported (Theisen et al., 2018), in vitro cross-presentation of sOVA was slightly reduced in *Wdfy4*$^{-/-}$ cDC1 compared with WT cDC1, but it was unaffected in *Wdfy4*$^{-/-}$ cDC2 compared with WT cDC2 (Fig. 6 A). However, in vitro cross-presentation of OVA-IC shows a dependence on WDFY4 in both cDC1 and cDC2, with greatest dependence at lower antigen doses (Fig. 6 B). Furthermore, in vivo cross-presentation of OVA-IC is strongly WDFY4 dependent. Immunization with OVA-IC induce strong OT-I proliferation in WT and Δ32 mice but weaker OT-I proliferation in *Wdfy4*$^{-/-}$ mice (Fig. 6, C and D). Lastly, we generated a double knockout of Δ32 mice and *Wdfy4*$^{-/-}$ mice (Δ32;*Wdfy4*$^{-/-}$), where cDC2 and monocyte-derived cells develop, and they are all WDFY4 deficient. This allows us to test whether cDC2 cross-presentation of ICs is WDFY4 depedent in the absence of cDC1 by it comparing with Δ32 mice. Indeed, Δ32; *Wdfy4*$^{-/-}$ mice show significantly lower OT-I proliferation compared with Δ32 mice after OVA-IC immunization (Fig. 6, E and F). Together, these results suggest that cDC2, like cDC1, also utilize WDFY4 for cross-presentation both in vitro and in vivo when exposed to certain forms of antigen, such as IC.

We previously observed that the cross-presentation of cell-associated antigen mediated by moDCs did not require WDFY4 (Theisen et al., 2018). We therefore assessed whether cross-presentation of IC by moDC required WDFY4. However, in vitro cross-presentation of OVA-IC by moDCs is independent of WDFY4 at all doses tested (Fig. S5, A and B). These data strengthen the observation of WDFY4-dependent cross-presentation in cDCs and suggest that moDCs may use a different cross-presentation pathway from cDC subsets.

Discussion

In this study, we broadened the analysis of in vivo antigen processing by the distinct cDC1 and cDC2 subsets. Genetic models lacking cDC1 have shown their importance for in vivo cross-presentation to $CD8^+$ T cell antigens derived from tumors

Downloaded from http://rupress.org/jem/article-pdf/222/4/e20240955/1938722/jem_20240955.pdf by guest on 08 May 2026

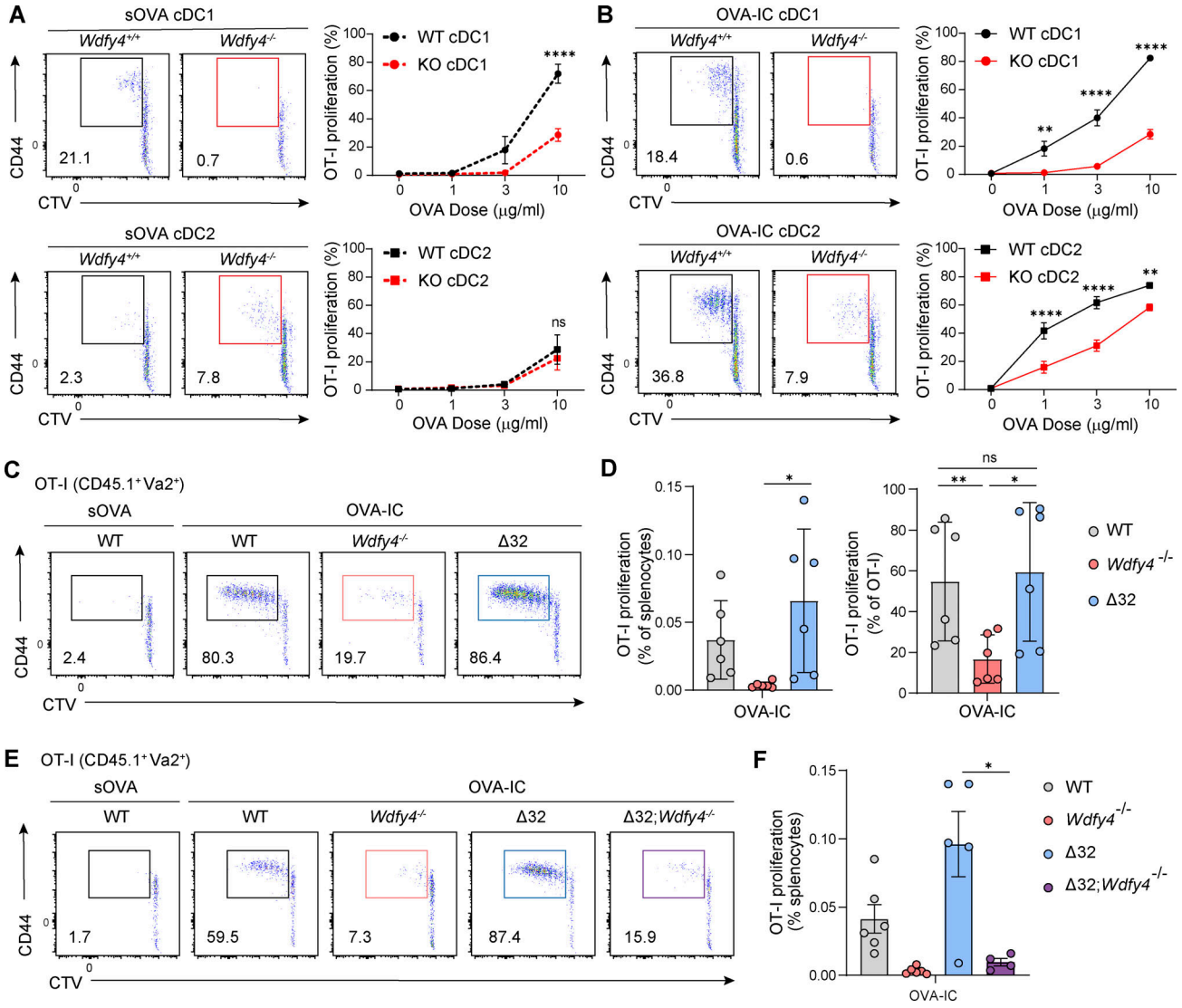

Figure 6. **cDC1 and cDC2 cross-presentation of IC is WDFY4 dependent. (A and B)** In vitro proliferation of OT-I cultured with cDC1 or cDC2 from WT or *Wdfy4*$^{-/-}$ mice and the indicated doses of sOVA (A) or OVA-IC (B). Representative histograms of OT-I proliferation are shown for 3 µg sOVA and 1 µg OVA-IC. Data are the mean ± SD for technical replicates of three independent experiments. Two-way ANOVA with Tukey's multiple comparisons test. **(C)** In vivo OT-I proliferation in WT, *Wdfy4*$^{-/-}$, and Δ32 mice on day 3 after intravenous immunization with 1 µg sOVA or OVA-IC. **(D)** Frequencies of OT-I proliferation from mice in C. Data represent mean ± SD of pooled biologically independent samples from two independent experiments (n = 6 for each genotype). **(E)** In vivo OT-I proliferation in WT, *Wdfy4*$^{-/-}$, Δ32, and Δ32; *Wdfy4*$^{-/-}$ mice on day 3 after intravenous immunization with 1 µg sOVA or OVA-IC. **(F)** Frequencies of OT-I proliferation from mice in E. Data represent mean ± SD of pooled biologically independent samples from two independent experiments (n = 4–6 for each genotype). Brown–Forsythe and Welch ANOVA with Dunnett's T3 multiple comparisons test. ns = not significant; *P < 0.05; **P < 0.01; ****P < 0.0001.

or viruses (Hildner et al., 2008; Durai et al., 2019). However, these studies did not address whether cDC1 also rely on other cells for antigen capture, as has been suggested (Ruhland et al., 2020; Jakubzick et al., 2013, 2017; Rawat et al., 2023). Specifically, cDC1-deficient mice can demonstrate a requirement for this subset in a response but cannot determine its sufficiency in that process or test the potential requirements for cDC2 or monocytes in acting as accessory cells in transferring antigen to cDC1. Furthermore, while cDC2 can cross-present antigen captured as ICs to CD8$^+$ T cells in vitro (den Haan and Bevan, 2002), testing this capacity in vivo requires genetic models that lack cDC2. Here, we combined several genetic models to evaluate the requirement and sufficiency of cDC1 and cDC2 as well as their reliance on accessory cells in the priming of CD4$^+$ and CD8$^+$ T cells in vivo in response to several forms of antigen.

First, we characterized cDC1- and cDC2-deficient mouse models to confirm that the remaining cDC subset faithfully reflect their respective cDC subset. We confirmed that the transcriptional profiles of cDC1 remaining in Δ1+2+3 mice and cDC2 remaining in Δ32 mice closely align with their counterparts present in WT mice. These results validate the use of these genetic models for probing the specific roles of cDC1 and cDC2 in a wide variety of conditions to examine the mechanisms by which these cells influence immune responses.

We also confirmed previous reports claiming a requirement for cDC1 in priming CD8$^+$ T cells with cell-associated antigens.

Downloaded from http://rupress.org/jem/article-pdf/222/4/e20240955/1938722/jem_20240955.pdf by guest on 08 May 2026

Using a newly developed Abelson-mOVA tumor model lacking MHC-I expression, we observed robust OT-I proliferation in vivo in response to antigen presentation by cDC1, but not cDC2, suggesting cDC1 are both necessary and sufficient for initiating $CD8^+$ T cell responses. Apart from cross-presentation, cross-dressing is an alternative pathway to cross-prime $CD8^+$ T cells with exogenous antigen whereby preformed peptide–MHC-I complexes from a donor cell are transferred directly to APCs (Chatterjee and Spranger, 2023). Our results with the Abelson-mOVA model exclude cross-dressing as the responsible mechanism for $CD8^+$ T cell priming, since Abelson-mOVA lack MHC-I expression. Notably, the capacity of cDC1 to prime $CD8^+$ T cells in vivo persisted in the absence of both cDC2 and monocytes, indicating that cDC1 are autonomously capable of antigen acquisition and processing of tumor-derived antigens, excluding previously suggested role of these cells as accessory cells in transferring antigens to cDC1.

We also extended earlier in vitro studies of antigens delivered as ICs (Baker et al., 2011; Boross et al., 2014; Ho et al., 2017) to an in vivo setting where the priming of $CD8^+$ and $CD4^+$ T cells can be definitively attributed to either cDC1 or cDC2. We find that both cDC1 and cDC2 are capable of cross-priming OT-I when immunized with OVA-IC in vivo, suggesting a potential use of preformed ICs in vaccination to enhance $CD8^+$ T cell responses. We also tested whether other APCs present in Δ32 mice, such as macrophages or moDCs, could cross-present OVA-IC to $CD8^+$ T cells. Using $\beta2m^{fl/fl}$ mice crossed with Cd11c-Cre^+ mice, we found a substantial loss of OT-I T cell proliferation in these mice when challenged with OVA-IC compared with WT control mice. In some models of viral infection and some tumors with high levels of type I IFN secretion, cross-dressing can be a mechanism by which cDC2 prime $CD8^+$ T cells due to effects of type I IFNs on cDC2 (Smyth et al., 2012; Bosteels et al., 2020; Duong et al., 2022). Here, in addition to cross-dressing by type I IFN stimulation, we show that cDC2 are also able to autonomously process OVA-IC onto MHC-I and cross-prime $CD8^+$ T cells in vivo, in a manner sufficient to induce $CD8^+$ T cell responses that can prevent tumor growth.

Another finding of this study is that different forms of OVA are differentially processed in vivo for presentation by MHC-I and MHC-II in cDC1 and cDC2. A previous study concluded that an intrinsic bias by cDC1 and cDC2 governed the OT-I proliferation in response to anti-DEC205–coupled antigen and OT-II proliferation to anti-DCIR2–coupled antigen (Dudziak et al., 2007). These results are compatible with the ability of the receptor to influence the route of antigen processing independently of cell type (Burgdorf et al., 2007; Kamphorst et al., 2010). For example, cDC1-specific receptor C-type lectin domain family 9 binds to exposed actin filaments from necrotic cells and favors MHC-I loading (cross-presentation) but is not required for internalization of antigen or loading of MHC-II from necrotic cells (Sancho et al., 2009; Ahrens et al., 2012; Zhang et al., 2012). Our data show that antigen presentation in vivo is influenced not only by intrinsic biases of cDC1 or cDC2 subsets but also by the form of antigen. Specifically, cell-associated antigen endows cDC1 not only with MHC-I processing but also with robust MHC-II–processing activity. ICs also enable cDC2 to process through both MHC-I and MHC-II pathways.

Heterogeneity within the cDC2 lineage includes Notch2-dependent support for Th17 responses (Satpathy et al., 2013) and Klf4-dependent support for Th2 responses (Tussiwand et al., 2015), corresponding with recent cDC2A and cDC2B nomenclature (Brown et al., 2019; Rodrigues et al., 2023; Minutti et al., 2024). A DC subset termed DC3 shares markers with conventional cDC2 but arises from $Ly6C^+$ monocyte-DC progenitors (Dutertre et al., 2019; Bourdely et al., 2020; Cytlak et al., 2020; Liu et al., 2023; Rodrigues et al., 2024). Importantly, Δ1+2+3 mice are depleted of all cDC2 and DC3 populations (Fig. S5 C). This present study did not differentiate the roles of these subsets in antigen presentation, but this may be of interest for future work.

Finally, we extended our understanding of the role of WDFY4. We observed that cross-presentation of IC was dependent on WDFY4 in both cDC1 and cDC2. This demonstrates an action of WDFY4 in cDC2 cells, which previously was shown only in cDC1 for the cross-presentation of cell-associated antigens. This finding was confirmed in WDFY4-deficient mice, which showed substantially reduced OT-I T cell proliferation in response to immunization with OVA–antibody complexes, especially at lower antigen doses. Cross-presentation by moDCs did not exhibit a similar dependency on WDFY4, suggesting that cDCs and moDCs utilize distinct pathways for processing and presenting complexed antigens. These findings underscore the importance of WDFY4 in the specialized antigen presentation functions of conventional DCs and point to potential avenues for modulating immune responses through targeted manipulation of this pathway.

Materials and methods

Mice

WT C57BL/6J (B6) (stock no. 000664), C57BL/6-Tg(TcraTcrb)1100Mb/J (OT-I) (stock no. 003831), C57BL/6Tg(TcraTcrb)425Cbn/J (OT-II) (stock no. 004194), and B6.SJL-Ptprca Pepcb/BoyJ (CD45.1) (stock no. 002014) were purchased from The Jackson Laboratory. OT-I and OT-II mice were bred to CD45.1 mice to produce CD45.1 OT-I and CD45.1 OT-II, respectively. C57BL/6NFWdfy4em1(IMPC)J/J ($Wdfy4^{-/-}$) (stock no. 029334) were generated as a part of KOMP2 project and obtained from The Jackson Laboratory. $Irf8\ +32^{-/-}$ mice (Δ32) (C57BL/6-Rr253em6Kmm/J, stock no. 032744; The Jackson Laboratory), which are homozygous for the deletion of the +32 kb Irf8 enhancer element, were generated in-house and described previously (Durai et al., 2019). Δ1+2+3 mice (C57BL/6-Rr253em6Kmm/J, stock no. 037704; The Jackson Laboratory), which are homozygous for three site mutations in the −165 kb zinc-finger E-box–binding homeobox 2 enhancer element, were generated in-house and described previously (Liu et al., 2022a). Δ32 mice were crossed to Δ1+2+3 mice to generate Δ32; Δ1+2+3 and characterized previously (Liu et al., 2022a). Mice harboring floxed alleles of β2-microglobulin ($\beta2m^{fl/fl}$) were crossed to Itgax-cre to generate conditional deletion of β2m on $CD11c^+$ cells. MHC-I TKO mice ($Kb^{-/-}Db^{-/-}\beta2m^{-/-}$) were originally provided by T. Hansen (Washington University, St. Louis, MO, USA) (Lybarger et al., 2003).

All mice were maintained in our specific-pathogen-free facility on 12-h light cycles and housed at 70°F and 50% humidity,

Downloaded from http://rupress.org/jem/article-pdf/222/4/e20240955/1938722/jem_20240955.pdf by guest on 08 May 2026

in accordance with institutional guidelines as well as with in vivo experiment procedures approved by the Association for Assessment and Accreditation of Laboratory Animal Care International–accredited Animal Studies Committee of Washington University in St. Louis following relevant ethical regulations.

Antibodies and flow cytometry

Flow cytometry and cell sorting were completed on an Aurora flow cytometer (Cytek) or a FACSAria Fusion instrument (BD). Flow cytometry data were collected using BD Facs-Diva software and analyzed with FlowJo analysis software. Surface staining was performed at 4°C in the presence of Fc block (2.4G2) in magnetic-activated cell-sorting (MACS) buffer (PBS + 0.5% BSA + 2mM EDTA). Biotinylated antibodies as follows were used to deplete cell population for efficient sort-purification of BM progenitors, splenic APCs, or OT-I and OT-II T cells. The following anti-mouse biotinylated antibodies were from Biolegend: B220 (RA3-6B2), Ly6G (1A8), CD3Ɛ (145-2C11), CD19 (6D5), TER119 (TER-119), CD8β (YTS156.7.7), and CD4 (GK1.5) antibodies. Biotinylated anti-mouse CD105 antibody (MJ7/18) was obtained from Invitrogen. BV650-conjugated streptavidin (405231) is from BioLegend. For fluorochrome-conjugated antibodies, the following anti-mouse antibodies are from BioLegend: AF488- and BV785-conjugated B220 (RA36B2; 103225 and 103246), AF647-conjugated Siglec H (551; 129608), BV510-conjugated I-A/E (M5/114.15.2; 100752), PE- and BV421-conjugated XCR1 (ZET; 148204 and 148216), PE-Cy7–conjugated CD24 (M1/69; 138508), APC-Cy7–conjugated Sirpα (P84; 110716), BV605- and BV510-conjugated CD8α (53-6.7; 100751 and 100752), APC-Cy7–conjugated CD45.1 (A20; 110716), PE-Cy7–conjugated CD45.2 (104; 109814), BV421-conjugated H-2Kb (AF6–88.5; 116525), PE-conjugated H-2Db (KH95; 111508), PE-conjugated Vα2 (B20.1; 127808), APC-conjugated CD44 (IM7; 103028 and), PerCP-Cy5.5–conjugated CD62L (MEL14; 104432), FITC-conjugated CD3Ɛ (145-2C11; 100306), FITC-conjugated CD11b (M1/70; 101206), BV711-conjugated CD4 (GK1.5; 100447), AF700-conjugated F4/80 (BM8, 123130), BV421-conjugated Ly6C (HK1.4; 128032), BV711-conjugated CD115/CSF-1R (AFS98; 135515), and APC-conjugated CD226 (10E5; 128810). The following anti-mouse antibodies are from BD Biosciences: BUV395-conjugated CD45R/B220 (RA3-6B2), BUV395-conjugated cKit (2B8), and PE-CF594–conjugated Flt3 (A2F10.1). The following anti-mouse antibodies are from Invitrogen: APC-eF780–conjugated CD44 (IM7), PE-Cy7–conjugated MerTK (DS5MMER), APC-eF780–conjugated CD11c (N418), and PerCP-ef710–conjugated Sirpα (P84).

Cell sorting

Naive OT-I cells were sorted from LNs and spleens of CD45.1 OT-I mice, as B220$^-$ CD45.1$^+$CD4$^-$CD8$^+$ Vα2$^+$ CD44$^-$ CD62L$^-$. Naive OT-II cells were sorted from the spleen of CD45.1 OT-II mice, as B220$^-$ CD45.1$^+$CD4$^+$CD8$^-$ Vα2$^+$ CD44$^-$ CD62L$^-$. cKit$^+$ BM progenitors were sorted as lineage$^-$ (CD3e, CD19, CD105, CD127, TER-119, Ly-6G, and B220) CD117$^+$. Splenic and FMS-like tyrosine kinase 3 ligand (Flt3L) DCs were sorted as B220$^-$MHC-II$^+$CD11c$^+$XCR1$^+$CD172α$^-$ (cDC1) and B220$^-$MHC-II$^+$CD11c$^+$XCR1$^-$CD172α$^+$ (cDC2). Macrophage/moDCs from the spleen were sorted as B220$^-$MerTK$^+$. Monocytes from the spleen were sorted as B220$^-$MHC-II$^-$CD11b$^+$CD115$^+$Ly6C$^+$.

DC preparation

For splenic DCs, spleens were minced and digested with 30 U/ml of DNase I (Sigma-Aldrich) and 250 µg/ml of collagenase B (Roche) in complete IMDM (Iscove's modified Dulbecco's medium with 2ME, non-essential amino acids, glutamine, penicillin/streptomycin, and 10% FBS) (I10F) for 30–45 min at 37°C with stirring. After digestion, single-cell suspension was passed through 70-µm strainers, and RBCs were lysed with ammonium chloride–potassium bicarbonate (ACK) lysis buffer. Cells were depleted of CD3e-, CD19-, TER-119–, Ly-6G–, and B220-expressing (lineage$^+$) cells by incubating with the corresponding biotinylated antibodies, followed by depletion with MagniSort Streptavidin Negative Selection Beads (Thermo Fisher Scientific).

For in vitro Flt3L-cultured DCs, tibias, femurs, and hips from mice were crushed into I10F to harvest BM cells. After RBC lysis using ACK lysis buffer, cells were depleted of CD3e-, CD19-, CD105-, CD127- TER-119–, Ly-6G–, and B220-expressing (lineage$^+$) cells by incubating with the corresponding biotinylated antibodies, followed by depletion with MagniSort Streptavidin Negative Selection Beads (Thermo Fisher Scientific). cKit$^+$ BM progenitors were sorted and cultured in I10F with 5% Flt3L-conditioned medium at 37°C. After 8 days, loosely adherent cells were harvested by pipetting.

Antigen preparation

sOVA was purchased from Worthington Biochemical Corporation and dissolved in PBS (1 mg/ml). OVA-IC was prepared as described previously (den Haan and Bevan, 2002). Briefly, Rabbit anti-OVA polyclonal IgG (Sigma-Aldrich) and sOVA were mixed at a concentration of 0.38 mg/ml OVA and 1.49 mg/ml anti-OVA in PBS and incubated for 30 min at 37°C.

For Abelson-mOVA, BM cells from MHC-I TKO (Kb$^{-/-}$ Db$^{-/-}$β2m$^{-/-}$) mice were harvested and transformed with Abelson murine leukemia virus (a gift from Barry Sleckman, University of Alabama at Birmingham, AL, USA). Abelson murine leukemia virus–transformed cell lines were then retrovirally transduced with MSCV-mOVA-IRES-Thy1.1 vector (Theisen et al., 2019) containing membrane OVA construct and sorted for Thy1.1$^+$ populations (Abelson-mOVA). Individual clones of Abelson-mOVA were generated by limited dilution cloning. Freeze-thawed Abelson-mOVA was used as a necrotic tumor antigen to standardize antigen quantity without growth. Briefly, 2 × 10^6 Abelson-mOVA cells were pelleted by centrifugation. After removing supernatant, cell pellet was quickly frozen at liquid nitrogen for 2 min and subsequently thawed at 37°C water bath for 2 min. The freeze-thaw cycles were repeated total of three times, and cell pellets were stored at −20°C until used. For antibody-coated Abelson-mOVA, freeze-thawed Abelson-mOVA cells were incubated with 1.49 mg/ml anti-OVA in PBS and incubated for 30 min at 37°C.

HKLM-OVA (a gift from H. Shen, University of Pennsylvania, Philadelphia, PA, USA) was prepared as previously described (Kretzer et al., 2016).

Downloaded from http://rupress.org/jem/article-pdf/222/4/e20240955/1938722/jem_20240955.pdf by guest on 08 May 2026

In vitro and in vivo antigen presentation assays

LNs and spleens from CD45.1 OT-I mice or CD45.1 OT-II mice were harvested and made into single-cell suspensions with mechanical separation followed by passing through 70-um strainers. After RBC removal using ACK lysis buffer, cells were depleted of TER-119–, I-A/E–, Ly-6G–, and B220-expressing cells by incubating with the corresponding biotinylated antibodies for 20 min at 4°C, followed by depletion with MagniSort Streptavidin Negative Selection Beads (Thermo Fisher Scientific). Naive OT-I or OT-II cells were sorted and labeled with cell trace violet (CTV) proliferation dyes (Thermo Fisher Scientific).

For in vitro cross-presentation assays, 2.5×10^4 CTV-labeled OT-I were co-cultured with sorted 1×10^4 cDC1, cDC2, monocyte, or macrophage/moDC without antigen or with 2.5×10^4 freeze-thawed Abelson-mOVA, 1×10^8 colony-forming units of HKLM-mOVA, or 100 µg/ml of sOVA, in a well of U-bottom 96-well plates. 3 days later, cells were washed with MACS buffer and analyzed for their CTV dilution and CD44 expression.

For in vivo antigen presentation assays, 5×10^5 CTV-labeled OT-I or OT-II cells were intravenously transferred into mice. 3 days later, spleens were harvested and depleted of RBC by ACK lysis, and CD45.1$^+$ OT-I or OT-II cells were analyzed for their CTV dilution and CD44 expression.

CD8$^+$ T cell tetramer staining

Spleens were minced, and single-cell suspension was passed through 70-µm strainers. After RBC lysis with ACK lysis buffer, cells were resuspended in MACS buffer. After cell counting by ViCell, 3–5 × 10^6 splenocytes were used for staining. APC- and PE-conjugated H-2Kb chicken OVA 257–264 SIINFEKL tetramers (National Institutes of Health Tetramer Core Facility) were added to the cells at a concentration of 1:100 in 10% Fc block (2.4g2) in MACS buffer and incubated at 37°C for 15 min. Subsequently, antibodies for surface staining were added without washing and incubated at 4°C for 30 min.

Tumor experiments

1956-mOVA was derived from the methylcholanthrene-induced fibrosarcoma 1956 tumor (a gift from Robert Schreiber, Washington University School of Medicine, St. Louis, MO, USA), as previously described (Theisen et al., 2019). It was generated in a female C57BL/6 mouse, tested for mycoplasma, and banked at low passage as previously described (Matsushita et al., 2012). Tumor cells derived from frozen stocks were propagated for 4–6 days in vitro with one intervening passage in RPMI media supplemented with 2ME, NEAA, glutamine, penicillin/streptomycin, and 10% FBS (R10F). On the day of injection, cells were harvested by trypsinization, washed three times with PBS, and resuspended at a density of 6.67×10^6 cells/ml. Mice were subcutaneously injected into the shaved flank with 10^6 cells. Tumor growth was measured every 3–5 days with a caliper. Two perpendicular diameters of tumor mass were measured and multiplied to calculate tumor area (mm^2). In accordance with our Institutional Animal Care and Use Committee–approved protocol, maximal tumor diameter was 20 mm, and in no experiments was this limit exceeded.

For immunization with CpG and anti-CD40 antibody per mouse, 5 µg of sOVA alone or preformed OVA-IC with 5 µg of sOVA, as described in "Antigen preparation," was mixed with 50 µg of CpG ODN1668 (Invivogen) and 100 µg of agonistic anti-CD40 antibody (clone FGK45; Leinco) into 150 µl injection in PBS. After 5 days, mice were subcutaneously injected into the shaved flank with 10^6 1956-mOVA in PBS. Tumor growth was measured every 3–5 days with a caliper. For immunization with CFA per mouse, 5 µg of sOVA alone or preformed OVA-IC with 5 µg of sOVA in 50 µl PBS was mixed with 50 µl of CFA (Becton Dickinson) and emulsified by vortex for 45 min. Mice were subcutaneously injected into the shaved flank with a 100 µl injection volume. After 5 days, mice were subcutaneously injected into the contralateral shaved flank with 10^6 1956-mOVA in PBS. Tumor growth was measured every 3–5 days with a caliper.

For CD8$^+$ T cell depletion, 200 µg of anti-mouse CD8b.2 antibody (clone 53–5.8; Leinco) was i.p. injected into mice. After 1 day, CD8$^+$ T cell depletion with <1% of remaining population was confirmed by cheek or tail bleeding and used for tumor experiments.

RRV infection experiment

9-week-old female WT and Δ32 mice were intravenously transferred 5×10^5 CTV-labeled OT-I cells, and, 24 h later, inoculated subcutaneously in the rear footpad with 10^3 focus-forming units of RRV (T48 strain) (Kuhn et al., 1991). 1 day after infection, 5×10^5 Abelson-mOVA cells were intravenously transferred. 4 days after infection, spleens and popliteal LNs were harvested and analyzed for DC populations and OT-I proliferation by flow cytometry.

Statistics

Statistical analyses were conducted using GraphPad Prism software version 10. All indicated center values indicate the mean, and all error bars correspond to the SDs unless otherwise specified. For groups that are not assumed to have equal variances, Welch and Brown–Forsythe one-way ANOVA was used.

RNA-seq and data analysis

Splenic cDC1s and cDC2s were sort purified as in "Dendritic cell preparation." Total RNA integrity was determined by Agilent Bioanalyzer or 4200 Tapestation. Libraries were prepared with 10 ng of total RNA using a Bioanalyzer RNA integrity number (RIN) score >8.0. Double stranded complementary DNA preparation was done by the SMARTer Ultra Low RNA kit for Illumina Sequencing (Takara-Clontech) as per the manufacturer's protocol and sequenced on an Illumina NovaSeq X Plus using paired-end reads extending 150 bases. Basecalls and demultiplexing were performed using Illumina's bcl2fastq software with a maximum of one mismatch in the indexing read.

RNA-seq reads were then aligned to the Ensembl release 101 primary assembly with STAR version 2.7.9a1. Gene counts were derived from the number of uniquely aligned unambiguous reads by Subread:featureCount version 2.0.32. Isoform expression of known Ensembl transcripts was quantified with Salmon version 1.5.23.

Online supplemental material

Fig. S1 compares the frequencies of cDCs and their progenitors in WT, Δ32, and Δ1+2+3 mice. Fig S2 shows the cross-presentation

Downloaded from http://rupress.org/jem/article-pdf/222/4/e20240955/1938722/jem_20240955.pdf by guest on 08 May 2026

of various forms of antigens by cDC1 versus cDC2. Fig S3 validates the selective depletion of MHC-I on cDCs from Cd11c-Cre; $\beta 2m^{fl/fl}$ mice. Fig S4 shows that immunization with ICs induces anti-tumor immunity in Δ32 mice. Fig S5 shows that WDFY4 is dispensable for in vitro cross-presentation of ICs by macrophage/moDCs.

Data availability

The RNA-seq data underlying Fig. 1 is openly available in the National Center for Biotechnology Information Gene Expression Omnibus database with the accession number GSE268380. All data in this study are available in the published article and its supplemental materials.

Acknowledgments

We thank J.M. White at the Department of Pathology and Immunology Transgenic Mouse Core at Washington University in St. Louis and the Genetic Editing and iPS Cell Center at Washington University in St. Louis for generating the mouse models. We thank the GTAC@MGI at Washington University School of Medicine for sequencing services. We thank the National Institutes of Health Tetramer Core Facility (contract number 75N93020D00005) for providing APC- and PE-conjugated H-$2K^b$ chicken OVA 257–264 SIINFEKL tetramers.

This work was supported by grants from the U.S. National Institutes of Health to K.M. Murphy (R01AI150297, R01CA248919, R01AI162643, and R21AI163421). J.L. Postoak, PhD, is supported by a Cancer Research Institute Irvington Postdoctoral Fellowship to Promote Racial Diversity (CRI5306).

Author contributions: S. Jo: conceptualization, data curation, formal analysis, investigation, methodology, project administration, resources, software, validation, visualization, and writing—original draft, review, and editing. R.A. Ohara: conceptualization, investigation, methodology, validation, and writing—review and editing. D.J. Theisen: conceptualization, data curation, investigation, methodology, and writing—review and editing. S. Kim: investigation, visualization, and writing—review and editing. T. Liu: methodology and resources. C.B. Bullock: investigation and methodology. M. He: formal analysis, investigation, and validation. F. Ou: investigation and resources. J. Chen: investigation, validation, visualization, and writing—original draft, review, and editing. S.J. Piersma: investigation and writing—review and editing. J.L. Postoak: investigation. W.M. Yokoyama: methodology, project administration, and resources. M.S. Diamond: conceptualization, funding acquisition, supervision, and writing—review and editing. T.L. Murphy: conceptualization, methodology, supervision, and writing—review and editing. K.M. Murphy: conceptualization, data curation, formal analysis, funding acquisition, methodology, project administration, resources, supervision, validation, and writing—original draft, review, and editing.

Disclosures: The authors declare no competing interests exist.

Submitted: 3 June 2024
Revised: 18 November 2024
Accepted: 17 January 2025

References

Ahrens, S., S. Zelenay, D. Sancho, P. Hanč, S. Kjær, C. Feest, G. Fletcher, C. Durkin, A. Postigo, M. Skehel, et al. 2012. F-actin is an evolutionarily conserved damage-associated molecular pattern recognized by DNGR-1, a receptor for dead cells. *Immunity*. 36:635–645. https://doi.org/10.1016/j.immuni.2012.03.008

Baker, K., S.-W. Qiao, T.T. Kuo, V.G. Aveson, B. Platzer, J.-T. Andersen, I. Sandlie, Z. Chen, C. de Haar, W.I. Lencer, et al. 2011. Neonatal Fc receptor for IgG (FcRn) regulates cross-presentation of IgG immune complexes by CD8-CD11b+ dendritic cells. *Proc. Natl. Acad. Sci. USA*. 108:9927–9932. https://doi.org/10.1073/pnas.1019037108

Bern, M.D., B.A. Parikh, L. Yang, D.L. Beckman, J. Poursine-Laurent, and W.M. Yokoyama. 2019. Inducible down-regulation of MHC class I results in natural killer cell tolerance. *J. Exp. Med.* 216:99–116. https://doi.org/10.1084/jem.20181076

Blander, J.M. 2023. Different routes of MHC-I delivery to phagosomes and their consequences to CD8 T cell immunity. *Semin. Immunol.* 66:101713. https://doi.org/10.1016/j.smim.2023.101713

Boross, P., N. van Montfoort, D.A.C. Stapels, C.E. van der Poel, C. Bertens, J. Meeldijk, J.H.M. Jansen, J.S. Verbeek, F. Ossendorp, R. Wubbolts, and J.H.W. Leusen. 2014. FcRγ-chain ITAM signaling is critically required for cross-presentation of soluble antibody-antigen complexes by dendritic cells. *J. Immunol.* 193:5506–5514. https://doi.org/10.4049/jimmunol.1302012

Bosteels, C., K. Neyt, M. Vanheerswynghels, M.J. van Helden, D. Sichien, N. Debeuf, S. De Prijck, V. Bosteels, N. Vandamme, L. Martens, et al. 2020. Inflammatory type 2 cDCs acquire features of cDC1s and macrophages to orchestrate immunity to respiratory virus infection. *Immunity*. 52:1039–1056.e9. https://doi.org/10.1016/j.immuni.2020.04.005

Bourdely, P., G. Anselmi, K. Vaivode, R.N. Ramos, Y. Missolo-Koussou, S. Hidalgo, J. Tosselo, N. Nuñez, W. Richer, A. Vincent-Salomon, et al. 2020. Transcriptional and functional analysis of CD1c+ human dendritic cells identifies a CD163+ subset priming CD8+CD103+ T cells. *Immunity*. 53:335–352.e8. https://doi.org/10.1016/j.immuni.2020.06.002

Brown, C.C., H. Gudjonson, Y. Pritykin, D. Deep, V.-P. Lavallée, A. Mendoza, R. Fromme, L. Mazutis, C. Ariyan, C. Leslie, et al. 2019. Transcriptional basis of mouse and human dendritic cell heterogeneity. *Cell*. 179:846–863.e24. https://doi.org/10.1016/j.cell.2019.09.035

Burgdorf, S., A. Kautz, V. Böhnert, P.A. Knolle, and C. Kurts. 2007. Distinct pathways of antigen uptake and intracellular routing in CD4 and CD8 T cell activation. *Science*. 316:612–616. https://doi.org/10.1126/science.1137971

Carbone, F.R., and M.J. Bevan. 1990. Class I-restricted processing and presentation of exogenous cell-associated antigen in vivo. *J. Exp. Med.* 171:377–387. https://doi.org/10.1084/jem.171.2.377

Chatterjee, F., and S. Spranger. 2023. MHC-dressing on dendritic cells: Boosting anti-tumor immunity via unconventional tumor antigen presentation. *Semin. Immunol.* 66:101710. https://doi.org/10.1016/j.smim.2023.101710

Cullinane, A.R., A.A. Schäffer, and M. Huizing. 2013. The BEACH is hot: A LYST of emerging roles for BEACH-domain containing proteins in human disease. *Traffic*. 14:749–766. https://doi.org/10.1111/tra.12069

Cytlak, U., A. Resteu, S. Pagan, K. Green, P. Milne, S. Maisuria, D. McDonald, G. Hulme, A. Filby, B. Carpenter, et al. 2020. Differential IRF8 transcription factor requirement defines two pathways of dendritic cell development in humans. *Immunity*. 53:353–370.e8. https://doi.org/10.1016/j.immuni.2020.07.003

Dudziak, D., A.O. Kamphorst, G.F. Heidkamp, V.R. Buchholz, C. Trumpfheller, S. Yamazaki, C. Cheong, K. Liu, H.-W. Lee, C.G. Park, et al. 2007. Differential antigen processing by dendritic cell subsets in vivo. *Science*. 315:107–111. https://doi.org/10.1126/science.1136080

Duong, E., T.B. Fessenden, E. Lutz, T. Dinter, L. Yim, S. Blatt, A. Bhutkar, K.D. Wittrup, and S. Spranger. 2022. Type I interferon activates MHC class I-dressed CD11b$^+$ conventional dendritic cells to promote protective anti-tumor CD8$^+$ T cell immunity. *Immunity*. 55:308–323.e9. https://doi.org/10.1016/j.immuni.2021.10.020

Durai, V., P. Bagadia, J.M. Granja, A.T. Satpathy, D.H. Kulkarni, J.T. Davidson IV, R. Wu, S.J. Patel, A. Iwata, T.-T. Liu, et al. 2019. Cryptic activation of an Irf8 enhancer governs cDC1 fate specification. *Nat. Immunol.* 20:1161–1173. https://doi.org/10.1038/s41590-019-0450-x

Durai, V., and K.M. Murphy. 2016. Functions of murine dendritic cells. *Immunity*. 45:719–736. https://doi.org/10.1016/j.immuni.2016.10.010

Dutertre, C.-A., E. Becht, S.E. Irac, A. Khalilnezhad, V. Narang, S. Khalilnezhad, P.Y. Ng, L.L. van den Hoogen, J.Y. Leong, B. Lee, et al. 2019.

Downloaded from http://rupress.org/jem/article-pdf/222/4/e20240955/1938722/jem_20240955.pdf by guest on 08 May 2026

Single-cell analysis of human mononuclear phagocytes reveals subset-defining markers and identifies circulating inflammatory dendritic cells. *Immunity*. 51:573–589.e8. https://doi.org/10.1016/j.immuni.2019.08.008

Ferris, S.T., V. Durai, R. Wu, D.J. Theisen, J.P. Ward, M.D. Bern, J.T. Davidson IV, P. Bagadia, T. Liu, C.G. Briseño, et al. 2020. cDC1 prime and are licensed by CD4+ T cells to induce anti-tumour immunity. *Nature*. 584: 624–629. https://doi.org/10.1038/s41586-020-2611-3

Gautier, E.L., T. Shay, J. Miller, M. Greter, C. Jakubzick, S. Ivanov, J. Helft, A. Chow, K.G. Elpek, S. Gordonov, et al. 2012. Gene-expression profiles and transcriptional regulatory pathways that underlie the identity and diversity of mouse tissue macrophages. *Nat. Immunol.* 13:1118–1128. https://doi.org/10.1038/ni.2419

Guilliams, M., F. Ginhoux, C. Jakubzick, S.H. Naik, N. Onai, B.U. Schraml, E. Segura, R. Tussiwand, and S. Yona. 2014. Dendritic cells, monocytes and macrophages: A unified nomenclature based on ontogeny. *Nat. Rev. Immunol.* 14:571–578. https://doi.org/10.1038/nri3712

den Haan, J.M., S.M. Lehar, and M.J. Bevan. 2000. CD8(+) but not CD8(-) dendritic cells cross-prime cytotoxic T cells in vivo. *J. Exp. Med.* 192: 1685–1696. https://doi.org/10.1084/jem.192.12.1685

den Haan, J.M.M., and M.J. Bevan. 2002. Constitutive versus activation-dependent cross-presentation of immune complexes by CD8(+) and CD8(-) dendritic cells in vivo. *J. Exp. Med.* 196:817–827. https://doi.org/10.1084/jem.20020295

Haist, K.C., K.S. Carpentier, B.J. Davenport, and T.E. Morrison. 2021. Plasmacytoid dendritic cells mediate control of Ross River virus infection via a type I interferon-dependent, MAVS-independent mechanism. *J. Virol.* 95:e01538-20. https://doi.org/10.1128/JVI.01538-20

Hildner, K., B.T. Edelson, W.E. Purtha, M. Diamond, H. Matsushita, M. Kohyama, B. Calderon, B.U. Schraml, E.R. Unanue, M.S. Diamond, et al. 2008. Batf3 deficiency reveals a critical role for CD8alpha+ dendritic cells in cytotoxic T cell immunity. *Science*. 322:1097–1100. https://doi.org/10.1126/science.1164206

Ho, N.I., M.G.M. Camps, E.F.E. de Haas, L.A. Trouw, J.S. Verbeek, and F. Ossendorp. 2017. C1q-dependent dendritic cell cross-presentation of in vivo-formed antigen-antibody complexes. *J. Immunol.* 198:4235–4243. https://doi.org/10.4049/jimmunol.1602169

Jakubzick, C., E.L. Gautier, S.L. Gibbings, D.K. Sojka, A. Schlitzer, T.E. Johnson, S. Ivanov, Q. Duan, S. Bala, T. Condon, et al. 2013. Minimal differentiation of classical monocytes as they survey steady-state tissues and transport antigen to lymph nodes. *Immunity*. 39:599–610. https://doi.org/10.1016/j.immuni.2013.08.007

Jakubzick, C.V., G.J. Randolph, and P.M. Henson. 2017. Monocyte differentiation and antigen-presenting functions. *Nat. Rev. Immunol.* 17: 349–362. https://doi.org/10.1038/nri.2017.28

Kamphorst, A.O., P. Guermonprez, D. Dudziak, and M.C. Nussenzweig. 2010. Route of antigen uptake differentially impacts presentation by dendritic cells and activated monocytes. *J. Immunol.* 185:3426–3435. https://doi.org/10.4049/jimmunol.1001205

Kretzer, N.M., D.J. Theisen, R. Tussiwand, C.G. Briseño, G.E. Grajales-Reyes, X. Wu, V. Durai, J. Albring, P. Bagadia, T.L. Murphy, and K.M. Murphy. 2016. RAB43 facilitates cross-presentation of cell-associated antigens by CD8α+ dendritic cells. *J. Exp. Med.* 213:2871–2883. https://doi.org/10.1084/jem.20160597

Kuhn, R.J., H.G. Niesters, Z. Hong, and J.H. Strauss. 1991. Infectious RNA transcripts from Ross River virus cDNA clones and the construction and characterization of defined chimeras with Sindbis virus. *Virology*. 182: 430–441. https://doi.org/10.1016/0042-6822(91)90584-X

Lehmann, C.H.K., A. Baranska, G.F. Heidkamp, L. Heger, K. Neubert, J.J. Lühr, A. Hoffmann, K.C. Reimer, C. Brückner, S. Beck, et al. 2017. DC subset-specific induction of T cell responses upon antigen uptake via Fcγ receptors in vivo. *J. Exp. Med.* 214:1509–1528. https://doi.org/10.1084/jem.20160951

Liu, K., and M.C. Nussenzweig. 2010. Origin and development of dendritic cells. *Immunol. Rev.* 234:45–54. https://doi.org/10.1111/j.0105-2896.2009.00879.x

Liu, T.-T., S. Kim, P. Desai, D.-H. Kim, X. Huang, S.T. Ferris, R. Wu, F. Ou, T. Egawa, S.J. Van Dyken, et al. 2022a. Ablation of cDC2 development by triple mutations within the Zeb2 enhancer. *Nature*. 607:142–148. https://doi.org/10.1038/s41586-022-04866-z

Liu, X., A. Taylor, Y.S. Poo, W.H. Ng, L.J. Herrero, P.C.H. Tang, A. Zaid, and S. Mahalingam. 2022b. TIR-domain-containing adapter-inducing interferon-β (TRIF)-dependent antiviral responses protect mice against Ross River virus disease. *MBio*. 13:e0336321. https://doi.org/10.1128/mbio.03363-21

Liu, Z., H. Wang, Z. Li, R.J. Dress, Y. Zhu, S. Zhang, D. De Feo, W.T. Kong, P. Cai, A. Shin, et al. 2023. Dendritic cell type 3 arises from Ly6C+ monocyte-dendritic cell progenitors. *Immunity*. 56:1761–1777.e6. https://doi.org/10.1016/j.immuni.2023.07.001

Lybarger, L., X. Wang, M.R. Harris, H.W. Virgin IV, and T.H. Hansen. 2003. Virus subversion of the MHC class I peptide-loading complex. *Immunity*. 18:121–130. https://doi.org/10.1016/S1074-7613(02)00509-5

Matsushita, H., M.D. Vesely, D.C. Koboldt, C.G. Rickert, R. Uppaluri, V.J. Magrini, C.D. Arthur, J.M. White, Y.-S. Chen, L.K. Shea, et al. 2012. Cancer exome analysis reveals a T-cell-dependent mechanism of cancer immunoediting. *Nature*. 482:400–404. https://doi.org/10.1038/nature10755

Min, J., D. Yang, M. Kim, K. Haam, A. Yoo, J.-H. Choi, B.U. Schraml, Y.S. Kim, D. Kim, and S.-J. Kang. 2018. Inflammation induces two types of inflammatory dendritic cells in inflamed lymph nodes. *Exp. Mol. Med.* 50: e458. https://doi.org/10.1038/emm.2017.292

Minutti, C.M., C. Piot, M. Pereira da Costa, P. Chakravarty, N. Rogers, H. Huerga Encabo, A. Cardoso, J. Loong, G. Bessou, C. Mionnet, et al. 2024. Distinct ontogenetic lineages dictate cDC2 heterogeneity. *Nat. Immunol.* 25:448–461. https://doi.org/10.1038/s41590-024-01745-9

van Montfoort, N., J.M.H. de Jong, D.H. Schuurhuis, E.I.H. van der Voort, M.G.M. Camps, T.W.J. Huizinga, C. van Kooten, M.R. Daha, J.S. Verbeek, F. Ossendorp, and R.E.M. Toes. 2007. A novel role of complement factor C1q in augmenting the presentation of antigen captured in immune complexes to CD8+ T lymphocytes. *J. Immunol.* 178:7581–7586. https://doi.org/10.4049/jimmunol.178.12.7581

Ohara, R.A., and K.M. Murphy. 2023a. The evolving biology of cross-presentation. *Semin. Immunol.* 66:101711. https://doi.org/10.1016/j.smim.2023.101711

Ohara, R.A., and K.M. Murphy. 2023b. Recent progress in type 1 classical dendritic cell cross-presentation - cytosolic, vacuolar, or both? *Curr. Opin. Immunol.* 83:102350. https://doi.org/10.1016/j.coi.2023.102350

Rawat, K., A. Tewari, X. Li, A.B. Mara, W.T. King, S.L. Gibbings, C.F. Nnam, F.W. Kolling, B.N. Lambrecht, and C.V. Jakubzick. 2023. CCL5-producing migratory dendritic cells guide CCR5+ monocytes into the draining lymph nodes. *J. Exp. Med.* 220:e20222129. https://doi.org/10.1084/jem.20222129

Rodrigues, P.F., A. Kouklas, G. Cvijetic, N. Bouladoux, M. Mitrovic, J.V. Desai, D.S. Lima-Junior, M.S. Lionakis, Y. Belkaid, R. Ivanek, and R. Tussiwand. 2023. pDC-like cells are pre-DC2 and require KLF4 to control homeostatic CD4 T cells. *Sci. Immunol.* 8:eadd4132. https://doi.org/10.1126/sciimmunol.add4132

Rodrigues, P.F., T. Trsan, G. Cvijetic, D. Khantakova, S.K. Panda, Z. Liu, F. Ginhoux, M. Cella, and M. Colonna. 2024. Progenitors of distinct lineages shape the diversity of mature type 2 conventional dendritic cells. *Immunity*. 57:1567–1585.e5. https://doi.org/10.1016/j.immuni.2024.05.007

Ruhland, M.K., E.W. Roberts, E. Cai, A.M. Mujal, K. Marchuk, C. Beppler, D. Nam, N.K. Serwas, M. Binnewies, and M.F. Krummel. 2020. Visualizing synaptic transfer of tumor antigens among dendritic cells. *Cancer Cell*. 37:786–799.e5. https://doi.org/10.1016/j.ccell.2020.05.002

Sancho, D., O.P. Joffre, A.M. Keller, N.C. Rogers, D. Martínez, P. Hernanz-Falcón, I. Rosewell, and C. Reis e Sousa. 2009. Identification of a dendritic cell receptor that couples sensing of necrosis to immunity. *Nature*. 458:899–903. https://doi.org/10.1038/nature07750

Satpathy, A.T., C.G. Briseño, J.S. Lee, D. Ng, N.A. Manieri, W. Kc, X. Wu, S.R. Thomas, W.-L. Lee, M. Turkoz, et al. 2013. Notch2-dependent classical dendritic cells orchestrate intestinal immunity to attaching-and-effacing bacterial pathogens. *Nat. Immunol.* 14:937–948. https://doi.org/10.1038/ni.2679

Shabman, R.S., K.M. Rogers, and M.T. Heise. 2008. Ross River virus envelope glycans contribute to type I interferon production in myeloid dendritic cells. *J. Virol.* 82:12374–12383. https://doi.org/10.1128/JVI.00985-08

Smyth, L.A., C. Hervouet, T. Hayday, P.D. Becker, R. Ellis, R.I. Lechler, G. Lombardi, and L.S. Klavinskis. 2012. Acquisition of MHC:peptide complexes by dendritic cells contributes to the generation of antiviral CD8+ T cell immunity in vivo. *J. Immunol.* 189:2274–2282. https://doi.org/10.4049/jimmunol.1200664

Theisen, D.J., J.T. Davidson IV, C.G. Briseño, M. Gargaro, E.J. Lauron, Q. Wang, P. Desai, V. Durai, P. Bagadia, J.R. Brickner, et al. 2018. WDFY4 is required for cross-presentation in response to viral and tumor antigens. *Science*. 362:694–699. https://doi.org/10.1126/science.aat5030

Theisen, D.J., S.T. Ferris, C.G. Briseño, N. Kretzer, A. Iwata, K.M. Murphy, and T.L. Murphy. 2019. Batf3-Dependent genes control tumor rejection induced by dendritic cells independently of cross-presentation. *Cancer Immunol. Res.* 7:29–39. https://doi.org/10.1158/2326-6066.CIR-18-0138

Downloaded from http://rupress.org/jem/article-pdf/222/4/e20240955/1938722/jem_20240955.pdf by guest on 08 May 2026

Tussiwand, R., B. Everts, G.E. Grajales-Reyes, N.M. Kretzer, A. Iwata, J. Bagaitkar, X. Wu, R. Wong, D.A. Anderson, T.L. Murphy, et al. 2015. Klf4 expression in conventional dendritic cells is required for T helper 2 cell responses. *Immunity*. 42:916–928. https://doi.org/10.1016/j.immuni.2015.04.017

Tussiwand, R., W.-L. Lee, T.L. Murphy, M. Mashayekhi, W. Kc, J.C. Albring, A.T. Satpathy, J.A. Rotondo, B.T. Edelson, N.M. Kretzer, et al. 2012. Compensatory dendritic cell development mediated by BATF-IRF interactions. *Nature*. 490:502–507. https://doi.org/10.1038/nature11531

Wu, R., R.A. Ohara, S. Jo, T.-T. Liu, S.T. Ferris, F. Ou, S. Kim, D.J. Theisen, D.A. Anderson III, B.W. Wong, et al. 2022. Mechanisms of CD40-dependent cDC1 licensing beyond costimulation. *Nat. Immunol.* 23:1536–1550. https://doi.org/10.1038/s41590-022-01324-w

Zhang, J.-G., P.E. Czabotar, A.N. Policheni, I. Caminschi, S.S. Wan, S. Kitsoulis, K.M. Tullett, A.Y. Robin, R. Brammananth, M.F. van Delft, et al. 2012. The dendritic cell receptor Clec9A binds damaged cells via exposed actin filaments. *Immunity*. 36:646–657. https://doi.org/10.1016/j.immuni.2012.03.009

Downloaded from http://rupress.org/jem/article-pdf/222/4/e20240955/1938722/jem_20240955.pdf by guest on 08 May 2026

Supplemental material

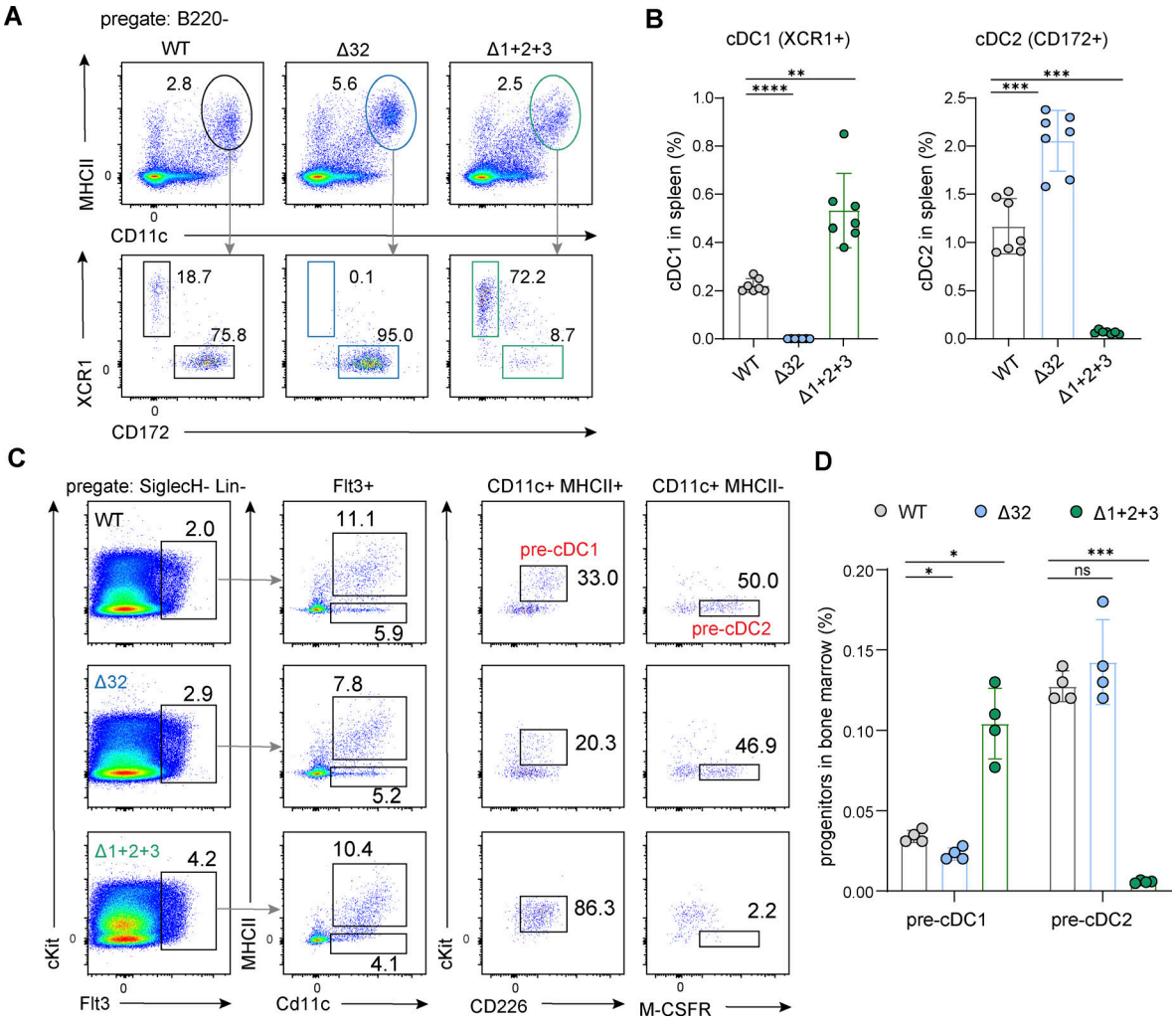

Figure S1. **Comparison of cDC1 and cDC2 in *Δ32* and *Δ1+2+3* mice. (A and B)** Representative flow plots (A) and frequencies (B) of splenic cDC1 and cDC2 in WT, *Δ32*, and *Δ1+2+3* mice. **(C and D)** Representative flow plots (C) and frequencies (D) of BM cDC progenitors in WT, *Δ32*, and *Δ1+2+3* mice. Numbers are the percentage of cells in the indicated gates. Data are mean ± SD of pooled biologically independent samples from two independent experiments (n = 7 in B and n = 4 in D). **(B and D)** Brown–Forsythe and Welch ANOVA with Dunnett's T3 multiple comparisons test. ns = not significant; *P < 0.05; **P < 0.01; ***P < 0.001; ****P < 0.0001.

Downloaded from http://rupress.org/jem/article-pdf/222/4/e20240955/1938722/jem_20240955.pdf by guest on 08 May 2026

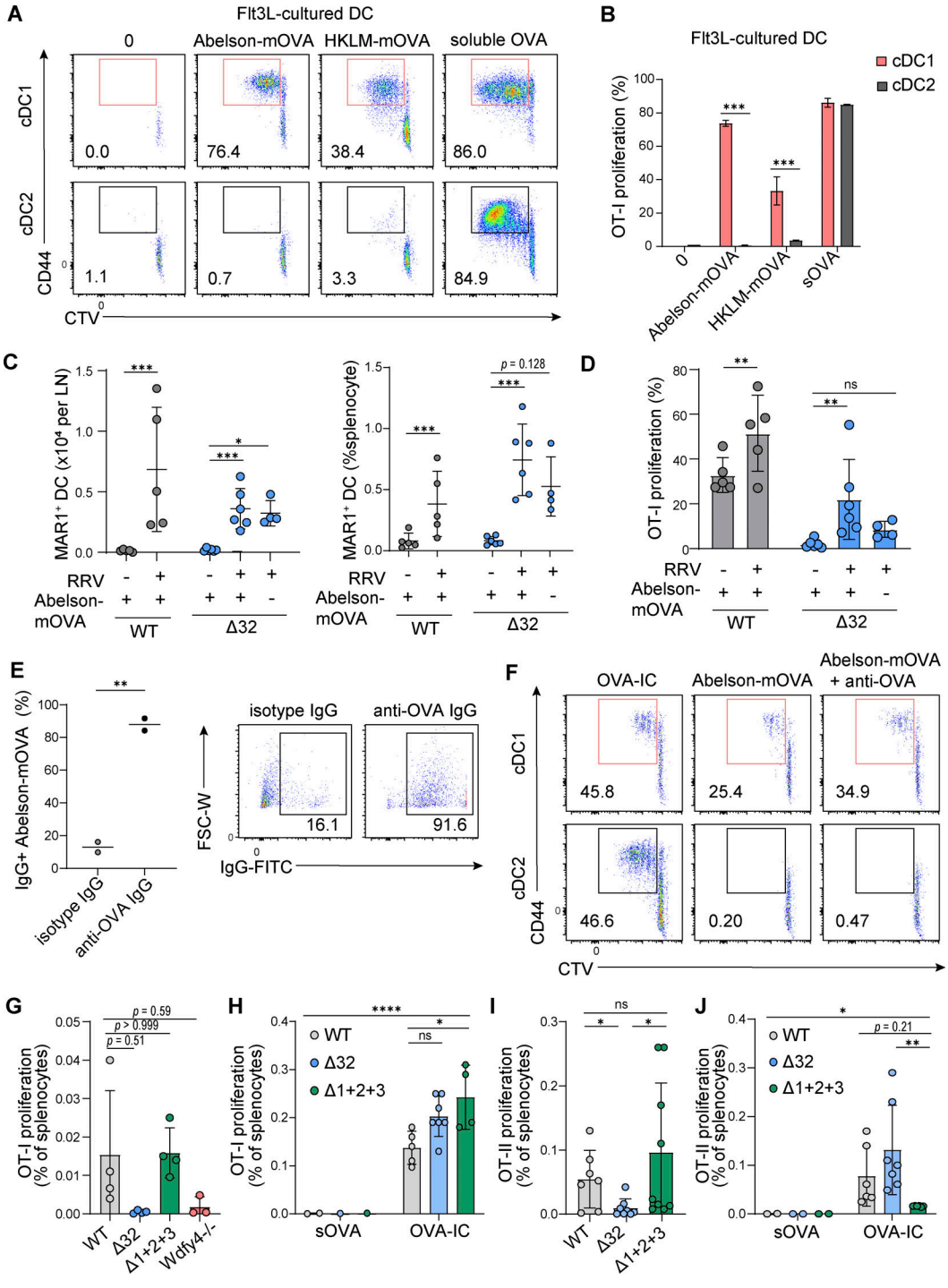

Figure S2. **IC antigens are efficiently cross-presented in vivo by both cDC1 and cDC2. (A)** In vitro proliferation of OT-I cultured with 1.25 × 10^4 cDC1 or cDC2 generated from BM in the presence of Flt3L, either alone or with 2.5 × 10^4 Abelson-mOVA cells, 10^8 HKLM-OVA, or sOVA (100 µg/ml). Numbers represent the percent of cells in the indicated gates. **(B)** Percent OT-I proliferation from A averaged for two independent experiments. Multiple *t* tests. **(C and D)** WT and Δ32 mice were injected with OT-I and immunized with Abelson-mOVA 1 day after RRV infection. 3 days later, spleen and draining inguinal LN were analyzed for DCs and OT-I populations. Data are the mean ± SD for technical replicates of two independent experiments. Two-way ANOVA with Tukey's multiple comparisons test. **(C)** Percentage of live $CD11c^+$ $MHCII^+$ $MAR\text{-}1^+$ $CD64^+$ cells in popliteal LN (left) and in spleen (right). **(D)** Percentage OT-I proliferation in spleen. **(E)** Percentage (left) and the representative plots (right) of IgG^+ Abelson-mOVA after preincubation either with isotype IgG or with anti-OVA IgG from two independent experiments. Unpaired *t* test. **(F)** Representative plot of Fig. 2 E. **(G)** Frequency of proliferating OT-I cells from Fig. 1, D and E shown as a percentage of total splenocytes. **(H)** Frequency of proliferating OT-1 cells from Fig. 2, A and B shown as a percentage of total splenocytes. **(I)** Frequency of proliferating OT-II cells from Fig. 4, A and B shown as a percentage of total splenocytes. **(J)** Frequency of proliferating OT-II cells from Fig. 4, C and D shown as a percentage of total splenocytes. **(F and H)** Brown–Forsythe and Welch ANOVA with Dunnett's T3 multiple comparisons test. **(G and I)** Two-way ANOVA with Tukey's multiple comparisons test. ns = not significant; *P < 0.05; **P < 0.01; ***P < 0.001; ****P < 0.0001. MAR-1: FceR1 α monoclonal antibody.

Downloaded from http://rupress.org/jem/article-pdf/222/4/e20240955/1938722/jem_20240955.pdf by guest on 08 May 2026

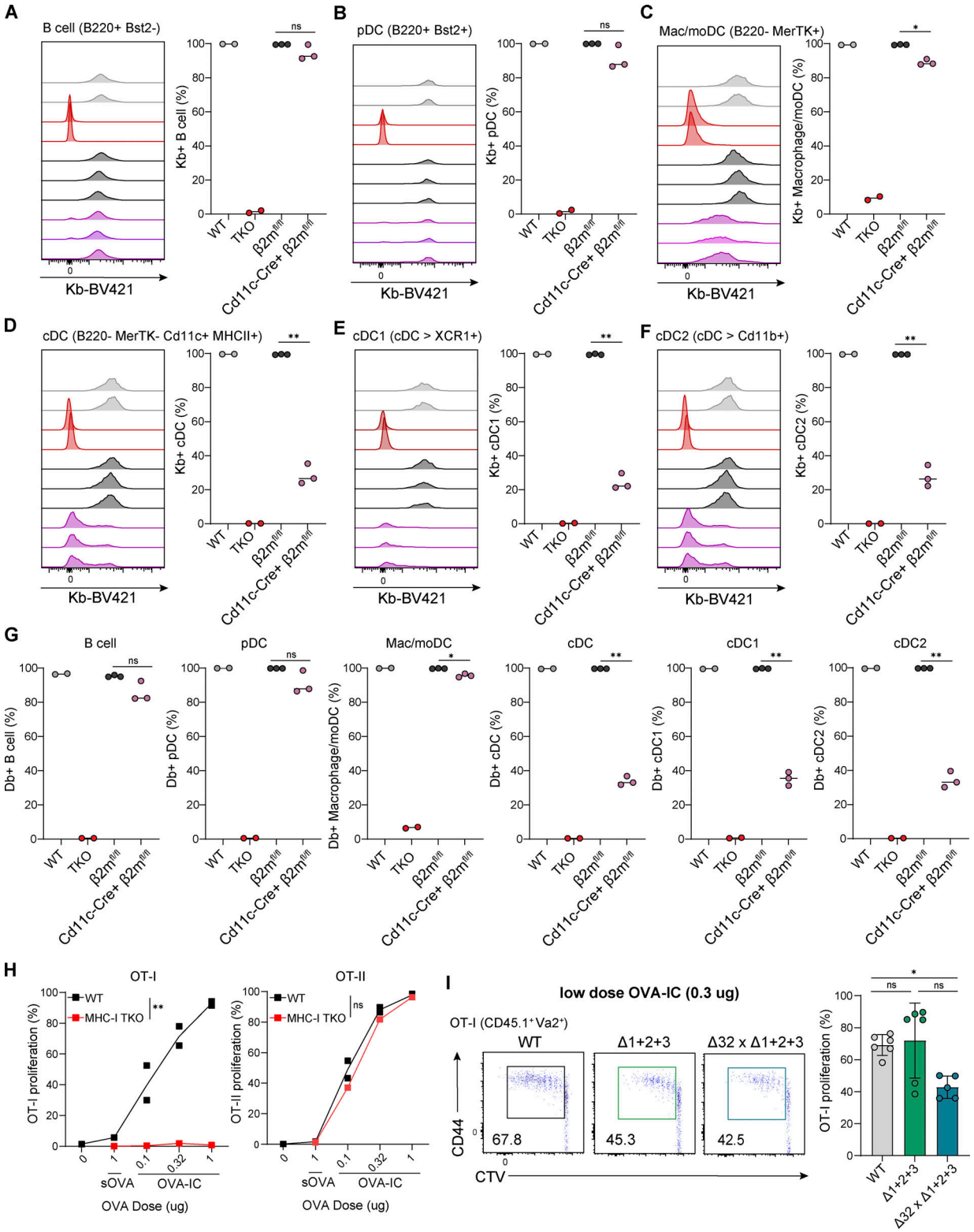

Figure S3. **Cd11c-Cre; β2m$^{fl/fl}$ mice selectively lack MHC-I on cDC1 and cDC2. (A–G)** Splenocytes from WT, MHC-I TKO (Kb$^{-/-}$ Db$^{-/-}$ β2m$^{-/-}$), β2m$^{fl/fl}$, and Cd11c-Cre^{+}; β2m$^{fl/fl}$ mice were analyzed for surface expression of H-2K^{b} (A–F) or of H2-K^{d} (G). Shown are histograms and frequency of K^{b+} cells for B cells (A), pDCs (B), macrophage/moDCs (C), total cDCs (D), cDC1s (E), and cDC2s (F). Data represent mean of pooled biologically independent samples (n = 2–3 for each genotype). Unpaired t test. **(H)** In vivo proliferation of OT-I and OT-II in WT or MHC-I TKO mice 3 days after intravenous immunization with the indicated dose of sOVA or OVA-IC. Data shown are from one representative experiment of two independent experiments with similar results. Ordinary two-way ANOVA. **(I)** In vivo OT-I proliferation in WT, Δ32, and Δ1+2+3 mice in response to low dose OVA-IC (0.3 µg per mouse.) Data are represented as mean values ± SD of pooled biologically independent samples from two independent experiments. Two-way ANOVA with Sidak's multiple comparisons test. ns = not significant; *P < 0.05; **P < 0.01.

Downloaded from http://rupress.org/jem/article-pdf/222/4/e20240955/1938722/jem_20240955.pdf by guest on 08 May 2026

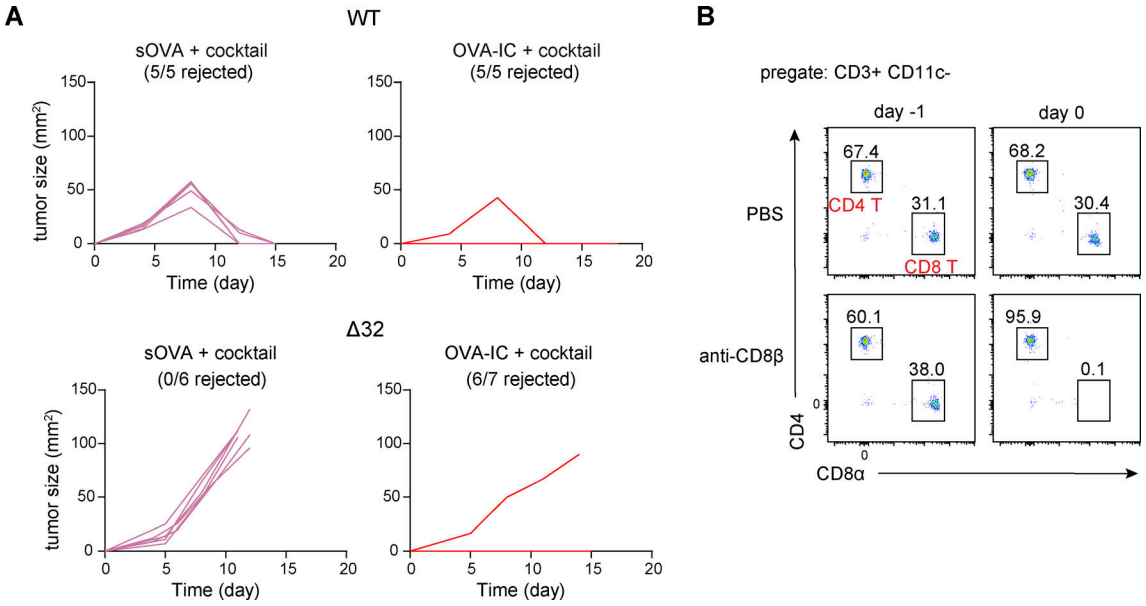

Figure S4. **Immunization with ICs induces anti-tumor immunity in *Irf8* Δ32 mice. (A)** Tumor growth from Fig. 5 A. **(B)** CD4⁺ and CD8α⁺ T cells were evaluated in peripheral blood before (day −1) or 1 day after (day 0) i.p. administration of 100 µg anti-CD8β antibody. Lymphocytes were pregated as CD3⁺ CD11c⁻ cells. Data shown are representative flow plots from two independent experiments.

Downloaded from http://rupress.org/jem/article-pdf/222/4/e20240955/1938722/jem_20240955.pdf by guest on 08 May 2026

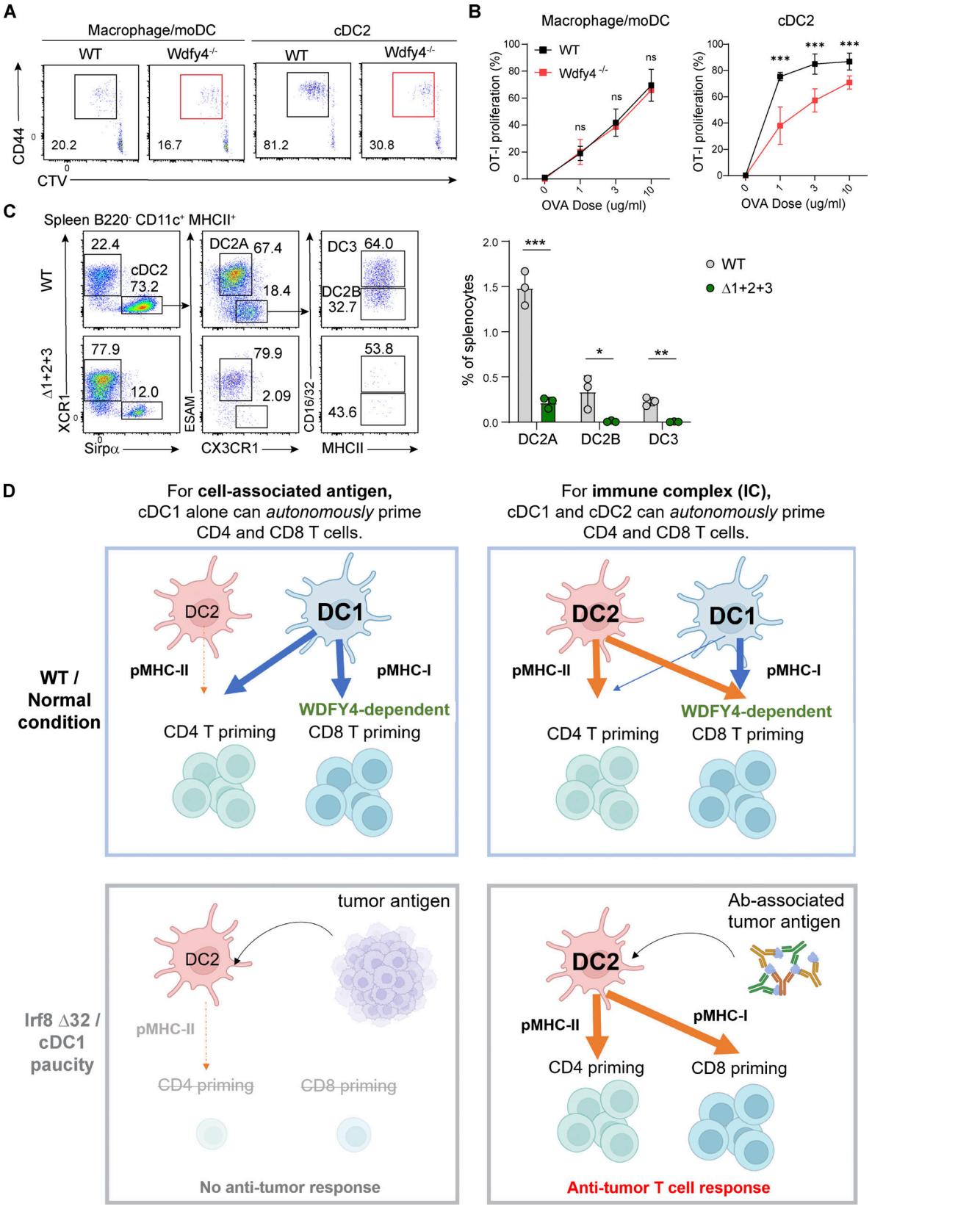

Figure S5. ***Wdfy4* is dispensable for in vitro cross-presentation of IC by macrophage/moDCs. (A)** In vitro proliferation of OT-I cultured for 3 days with macrophage/moDCs or cDC2 from WT and *Wdfy4*$^{-/-}$ mice and the indicated dose of OVA-IC. **(B)** Frequency of OT-I proliferation from A. Data represent mean ± SEM of two independent experiments. Two-way ANOVA with Sidak's multiple comparisons test. **(C)** Gating strategy (left) and the percentage in spleen (right) for cDC2a, cDC2b, and DC3s from spleen of WT or Δ1+2+3 mice. Pregated on live B220^{-} CD11c^{+} MHC-II^{+} population. Data are represented as mean values ± SD combined from two independent experiments. Multiple *t* tests. ns = not significant; *P < 0.05; **P < 0.01; ***P < 0.001. **(D)** Graphical abstract.

Downloaded from http://rupress.org/jem/article-pdf/222/4/e20240955/1938722/jem_20240955.pdf by guest on 08 May 2026